Ion Energy Distributions in Collisionless and Collisional, Capacitive RF Sheath

by

Ying Wang

A dissertation submitted in partial satisfaction of the
requirements for the degree of
Doctor of Philosophy

in

Engineering - Nuclear Engineering

in the

Graduate Division

of the

University of California, Berkeley

Committee in charge:

Professor John P. Verboncoeur, Chair
Professor Michael A. Lieberman
Professor Jasmina Vujic

Fall 2012

Ion Energy Distributions in Collisionless and Collisional, Capacitive RF Sheath

Abstract

Ion Energy Distributions in Collisionless and Collisional, Capacitive RF Sheath

by

Ying Wang

Doctor of Philosophy in Engineering - Nuclear Engineering

University of California, Berkeley

Professor John P. Verboncoeur, Chair

Capacitively driven radio frequency (rf) discharges are commonly used for plasma-assisted material processing. Because of the significant difference in the mobility of electrons and ions, a thin layer of sheath is always established at the boundary, which separates the discharge into two regions: quasi-neutral bulk plasma and positively charged sheath. Within the sheath, ions are accelerated by electric fields and therefore, bombard the electrode with significant energies. The ion energy distribution (IED) on the substrate is essentially important in the optimization of discharge operations. For plasmas sources typically operated at higher densities and lower pressures, the ion motion in the rf sheath is mainly collisionless since the ion mean free path is much larger than the sheath width. At high operating pressures and large sheath voltage drops, the sheaths are typically collisional.

A fast and simple model consisting of a series of computational steps is of great value to predict the plasma parameters and IEDs, given the control parameters of the discharge. Respective models for IEDs in collisionless and collisional capacitive rf sheaths are developed in this dissertation, based on the sheath models developed in late 1980s. Both models do not rely on any intermediate parameters from simulation or experimental results and only take a few seconds (collisionless) or minutes (collisional) to get the final IEDs. Ion-neutral charge exchange reactions are considered for collisional rf sheaths. Energy dependent ion mean free path is taken into account. Particle-in-cell (PIC) simulations are used to verify the previous sheath models and the IED models.

The PIC code OOPD1, being developed with a powerful capability as the development of the collisional IED model goes on, is introduced in this dissertation. Comparisons with XPDP1 are presented, which confirms OOPD1 as a trustable, friendly, and extensible simulation tool to observe the rf discharges.

To Mao Dan

Contents

List of Figures **iv**

List of Tables **vi**

1 Introduction to IEDs in Capacitive RF Sheath **1**
1.1 Introduction . . . 1
1.2 Motivation . . . 2
1.3 Previous Work . . . 3
1.4 Dissertation Overview . . . 5

2 Simulation Models **6**
2.1 XPDP1 . . . 7
2.2 OOPD1 . . . 7
2.3 Code Comparison . . . 8
2.3.1 Input file . . . 8
2.3.2 Speed . . . 9
2.3.3 Example . . . 9

3 Model of Collisionless Ion Energy Distributions **11**
3.1 Introduction . . . 11
3.2 Collisionless Sheath Model . . . 12
3.3 Collisionless IED Model . . . 12
3.4 Example . . . 12
3.5 PIC Simulation . . . 15
3.6 Results and Discussions . . . 15
3.7 Summary . . . 17

4 Collisional Sheath Model with Energy Dependent λ_i **24**
4.1 Introduction . . . 24
4.2 Basic Equations . . . 24
4.3 Sheath Capacitance . . . 34

4.4 Sheath Conductance 36
4.5 Example 37
4.6 Summary 37

5 IEDs in Collisional, Capacitive RF Sheath 39
5.1 Introduction 39
5.2 Collisional, Capacitive RF Sheath Model 41
5.2.1 Example 41
5.3 Collisional IED Model 42
5.3.1 Limitation 42
5.3.2 Scheme 43
5.3.3 Example 43
5.3.4 Normalization 48
5.3.5 Notes 48
5.4 PIC Simulation 50
5.4.1 Verification of Collisional RF Sheath Model by PIC 51
5.4.2 PIC Results of Collisional IEDs 54
5.4.3 Comparisons between theory and PIC 58
5.5 Summary 62
5.6 Future Work 62

6 Conclusion and Future Work 63
6.1 Conclusion 63
6.2 Future Work 64

List of Figures

1.1 Theory Model 3

2.1 Flow schematic for the PIC scheme. 7
2.2 IEDs from XPDP1 and OOPD1 for a single frequency driven capacitive discharge 10
2.3 IEDs from XPDP1 and OOPD1 for a dual-frequency driven capacitive discharge 10

3.1 Scheme for Alan Wu's semianalytical IED model 16
3.2 PIC time-averaged temperatures for $V_{rf} = 500V$ at 13.56 MHz 18
3.3 PIC time-averaged densities for $V_{rf} = 500V$ at 13.56 MHz 18
3.4 Theoretical, semianalytical, and PIC IEDs for $V_{rf} = 500V$ at 13.56 MHz . . 19
3.5 Theoretical, semianalytical, and PIC IEDs for $I_{rf} = 2.05A$ at 13.56 MHz . . 19
3.6 Theoretical IEDs for current-driven (top) and voltage-driven (bottom) discharges at 13.56 MHz 20
3.7 PIC IEDs for current-driven (top) and voltage-driven (bottom) discharges at 13.56 MHz 20
3.8 Theoretical IEDs for $V_{rf} = 500V$ at 6.78, 13.56, 27.12, and 40 MHz, respectively 21
3.9 PIC IEDs for $V_{rf} = 500V$ at 6.78, 13.56, 27.12, and 40 MHz, respectively . . 21

4.1 H/H_0 versus H_0 for varying b 27
4.2 H/H_0 versus b 28
4.3 Normalized position versus phase for varying b 29
4.4 Normalized C_{sm} versus b 29
4.5 C_{s0} versus b 30
4.6 Normalized dc electric field versus position for varying b 31
4.7 Normalized ion density n_i/n_0 versus position for varying b 31
4.8 Normalized dc potential Φ/T_e versus position for varying b 32
4.9 Normalized C_V versus b 33
4.10 Normalized sheath voltage versus phase for varying b 35
4.11 Normalized C_{Vm} versus b 35

5.1 Ion mean free path λ_i vs. ion velocity 40
5.2 IED from theory at $V_{rf} = 176$ V with various energy dependence of λ_i over v 49

5.3 Collisional IED from theory at $V_{rf} = 176$ V with various energy dependence of λ_i over v 50
5.4 IED from theory at $V_{rf} = 500$ V with various energy dependence of λ_i over v 51
5.5 Sheath width vs. time 52
5.6 Magnitude of sheath width vs. frequency 52
5.7 Sheath voltage vs. time 53
5.8 Magnitude of sheath voltage vs. frequency 53
5.9 Time-averaged temperature vs. position 54
5.10 Time-averaged potential vs. position 55
5.11 Time-averaged density vs. position 55
5.12 IED from PIC at $V_{rf} = 176$ V with f =81 MHz 56
5.13 IEDs from PIC at $V_{rf} = 500$ V with f =13.56 and 27.12 MHz 56
5.14 IED from PIC with different cutoff energies of fast neutrals ε 57
5.15 IED from PIC with/out ion-neutral elastic scattering collisions 58
5.16 IADs within sheath, from PIC 59
5.17 IEDs within sheath, from PIC 59
5.18 IEDs from theory and PIC at $V_{rf} = 176V$ 60
5.19 IEDs from theory and PIC at $V_{rf} = 500V$ 60
5.20 IEDs from theory and PIC with a constant λ_i 61
5.21 IEDs from theory and PIC with an energy dependent λ_i 61

List of Tables

2.1 Speed Comparison of XPDP1 and OOPD1 w/o XGrafix 9

3.1 Theoretical and Simulation Discharge Parameters 23

4.1 Coefficients of Fourier Series Expansion of $V(t)$ for Varying b 38
4.2 Some Parameters for Varying b 38

Acknowledgments

I've had a great time at Berkeley during my PhD program. I would not have had such a nice experience without the help and support from you:

Thank you, Professor Verboncoeur. You gave me the opportunity of studying at UC Berkeley. I still remember your words six years ago saying that "studying at UC Berkeley is a once-in-a-life-time opportunity". At the very end of the program, I'm completely convinced by you. When I was worried about my slow progress at the beginning, you comforted me, saying "there's always a learning curve, for anyone, for anything. You're doing a good job." Thank you for introducing me to Professor Lieberman to take on this interesting project. Thank you for all these years co-advising me with Professor Lieberman, continuing guiding me through a weekly Skype meeting even after you move to Michigan. Thank you for always being there whenever I gave a talk on a conference. With you nodding your head, I was less nervous and more confident. Every time I would hear you say, "Ying, that was a very nice talk!" Every time I would respond, "Really? I was so nervous..." I guess from all these years' experience, you must have found out that I'm not a confident person as you are. You've tried all the ways to help me establish my confidence. Thank you.

Thank you, Professor Lieberman. I've learned a lot from you. You started to learn C++ at your 70's. Now I'm using the code updated by you with the new programming skills you achieved. I don't know if I can be as hard working and curious as you when I'm at your age. I want to be someone like you. But it's way too difficult for me as I can imagine. You've no idea how much effects you've had on me. This is not only about your research attitude, creative ideas, sharp and precise minds, but also about how to be a good person with an honorable personality. I'm lucky to be your student.

Thank you, Professor Vujic. Thank you for serving as the committee member for my qualifying exam and dissertation. Thank you for sharing your personal experience of fighting with life as an adorable mother, a successful professor. Thank you for financially supporting me when our research funding ran out. Thank you for hooding me at the graduation ceremony. Thank you for understanding me as a mother and providing me with all the convenience, out of my expectation. Thank you for being so considerate and supportive. I would rather like to have gotten to know you earlier.

Thank you, Professor Lichtenberg for being on my qualifying exam committee.

Thank you, Lisa. You're my best student services adviser. Whenever I have questions, you have the answers. "Go talk to Lisa. She must know!" I cannot remember how many times I entered your office with concerns and anxieties, then left with a smile.

Thank you, Alan, my friend. Thank you for your good work on the project. It's my pleasure to take it over. Thank you for setting up my laptop, installing all the programs, and providing useful information whenever I run into computer problems.

Thank you, Professor Leung and Professor Bibber. Thank you for helping me on my job hunting.

Xiexie, Mama, Baba, Jiejie. Nimen shi zui ai wo de ren. Xiexie nimen dui wo he Maodan de guanxin zhaogu. Wo ai nimen!

Chapter 1

Introduction to IEDs in Capacitive RF Sheath

1.1 Introduction

Capacitive rf discharges are widely used in the fabrication of integrated circuits (IC) and plasma processes such as thin film deposition and surface modification. In these discharges, an rf voltage is applied to the driving electrode. Due to the big difference in mass, the mobile electrons respond to the instantaneous electric fields produced by the rf driving voltage, while the massive ions respond only to the time-averaged electric fields. This gives a picture of electrons oscillating back and forth within the positive space charge cloud of the ions, which creates sheath regions near each electrode as electrons are lost to the electrodes. Within the sheath, the positive charge exceeds the negative charge, with the excess charge producing a strong electric field within the sheath, pointing from the bulk plasma to the electrode. As ions flowing out of the bulk plasma enter the sheath zone with an initial velocity equal to the Bohm presheath velocity $u_B = (eT_e/M)^{1/2}$, they get accelerated by the sheath fields and pick up high energies as they traverse across the sheath. Here, T_e is the electron temperature (in volts) and M is the ion mass. The final energy that they carry to the electrode, known as the ion bombardment energy, plays an important role in determining the ion etch rates, selectivity and damage control in processing plasmas.

Within a collsionless sheath where the ion mean free path is much larger than the sheath width, ions are continuously accelerated by the sheath field. Ions pick up energies as they enter the plasma-sheath edge and bombard the substrate with an energy distribution of a bimodal shape. At low frequencies ($\tau_{ion}/\tau_{rf} << 1$), the ions cross the sheath in a small fraction of an rf cycle. Here, τ_{ion} is the time an ion takes to traverse the sheath and τ_{rf} is the rf period. The phase of the rf cycle at which ions enter the sheath determines their bombarding energy. In this case, the IED is broad and bimodal, with the two peaks corresponding to the minimum and maximum of the sheath drops. At high frequencies ($\tau_{ion}/\tau_{rf} >> 1$), it

takes the ions many rf cycles to cross the sheath. As a result, the ions respond only to the time-averaged sheath voltage. The effect of phase at which they enter the sheath is small. In this case, the IED is still bimodal, but much narrower. As τ_{ion}/τ_{rf} increases, the two peaks approach each other and may not be resolved [4, 11, 14, 15]. During the past 40 years, collisionless sheath models in single-frequency capacitive discharges have been developed [2, 29, 9, 30, 23], and the sheath dynamics at various frequencies have been studied [34, 31].

Within a collisional sheath where the ion mean free path is much smaller than the sheath width, ions have collisions with neutrals through charge exchange, elastic scattering and other reactions. Primary ions, defined as those ions entering the sheath edge from the bulk plasma, lose their energies through ion-neutral collisions. Secondary ions are created within the sheath and accelerated toward the substrate, also losing energy via collisions. Therefore, a large spread of the IED is observed with multiple peaks at low energies [43, 44, 24, 26, 28, 16, 5].

It is known as a crucial limit of capacitive rf discharges that the ion bombarding flux $\Gamma_i = n_0 u_B$ (n_0 is the number density of ions at the presheath-sheath edge) and bombarding energy E_i cannot be controlled independently, with a single frequency drive. Because of the ion flux conservation within the sheath, as ions being accelerated towards the substrate, their number density decreases with increasing velocity. After 1990, dual-frequency discharges have drawn much attention due to their independent control of the ion bombarding fluxes Γ_i and ion bombarding energies E_i at the substrates. Analytical [33] and semi-analytical [45] models were developed to better understand the mechanics in multi-frequency capacitive discharges. Numerical calculations and simulations have also been used [19, 8, 12, 45]. Although this dissertation only covers the single frequency drive, with a clear and better understanding of the sheath dynamics in a single frequency capacitively driven discharge, the work may be extended to dual- and multi-frequency as needed.

1.2 Motivation

Once a complete set of control parameters is given, for example, the power source (rf frequency f, driving voltage V_{rf} or current I_{rf}), the feedstock gas type, pressure p, and the geometry (the distance between electrodes L and the area of the electrodes A), the state of the discharge is specified, with the remaining plasma and circuit parameters determined as functions of the control parameters, among which the ion energy distribution (IED) is especially crucial. A diagram of the system is shown in Fig. 1.1.

Various models have been developed to calculate the IEDs in a single frequency rf sheath, for which either experimental results are needed as the input parameters of their models, or the sheath response from simulations is required. A simple and fast model which does not rely on any intermediate plasma parameters is lacking. This dissertation aims at developing simple and fast models consisting of series of computational steps to accurately predict IEDs from the control parameters. Since the IED is essentially determined by the sheath response,

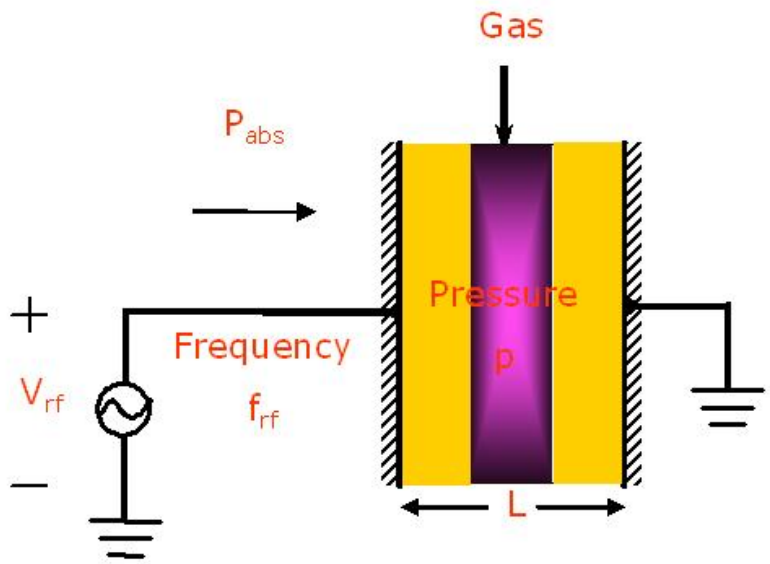

Figure 1.1: Theory Model

it is necessary to establish the relationship between the control parameters and the sheath response. Given the cost of time and money required by experiments and simulations, it is valuable to develop simple and fast models to better understand the physics of the discharge and more accurately predict the IED. The control parameters of the discharge are the only input parameters required by the models presented in this dissertation.

1.3 Previous Work

Many studies have been done in the past 40 years regarding the single frequency capacitive discharges. Some of the earlier works include [2, 38, 18, 21, 37, 22, 43, 44, 40, 35, 7, 1, 28, 6]. More recent works include [20, 46, 25, 16, 5]. Due to the complexity of the rf sheath dynamics, most of the calculations of IEDs rely on numerical methods. A complete self-consistent analytical model is quite complicated, even in the simplest plane-parallel geometry. Analytical expressions for IEDs are rare and only can be obtained by making various simplifying assumptions and limiting approximations. Among these studies, references [2, 6, 16, 5] calculate the IEDs by approximate analytical models. Numerical integration of the equations of motion [43, 44, 26, 38, 29, 7], Monte Carlo simulations [24, 18, 37, 1, 28] and particle-in-cell (PIC) simulations [40, 35, 36] have also been used to calculate the IEDs. Although most studies have been for argon, the IEDs in other gases such as oxygen and hydrogen have also been studied with more complex chemical reactions [3, 32, 27]. Comprehensive reviews of

the research on IEDs are presented in references [17, 10].

The studies in this dissertation are primarily based on the previous work of Lieberman's collsionless and collisional rf sheath models [21, 22] and Benoit-Cattin's collisionless IED model [2]. The collisionless sheath model gives an analytical, self-consistent solution for the collisionless rf sheath driven by a single frequency source. Given the control parameters of the discharge, the rf frequency f, driving voltage V_{rf} or current I_{rf}, the feedstock gas type, pressure p, and the geometry, this model provides a full set of expressions for the time-averaged ion and electron densities, electric field, and potential within the sheath. This model also provides the estimations of other plasma parameters such as sheath width, electron temperature, dissipated power, and mean ion bombarding energy, those of which are crucial parameters needed to predict the IED. Similarly, the later developed collisional sheath model provides a full set of expressions and estimations for the plasma parameters for the collisional rf sheath, driven by a single frequency source. The key assumption is that the ion motion is collisional, with the ion mean free path a constant within the sheath. The nonlinear oscillation motion of the electron sheath boundary and the nonlinear oscillating sheath voltage can be obtained by this analytical, self-consistent collisional rf sheath model. These two sheath models establish the relation between the control parameters and plasma parameters.

To calculate the IEDs, the sheath response is required to estimate the energies that ions pick up as they cross the sheath. Benoit-Cattin's collisionless IED model solves this problem in the high frequency regime ($\tau_{ion}/\tau_{rf} >> 1$). This model gives analytical expressions for the spread of ion bombarding energy and the IED by assuming a constant sheath width, a uniform sheath electric field, a sinusoidal sheath voltage, and zero initial ion velocity at the plasma-sheath boundary. It is found that the energy spread is directly proportional to τ_{rf}/τ_{ion}.

Ref.[45] provides a semi-analytical solution of the IED for multi-frequency capacitive rf discharges. With the time-varying functions of sheath response, sheath width and sheath voltage provided by particle-in-cell simulations, this model gives a fast and simple method of calculating IEDs based on a linear transfer function that relates the time-varying sheath voltage to the time-varying ion energy response at the surface. The transfer function, determined by τ_{rf}/τ_{ion}, acts as a filter that filters out the effects of the fast varying sheath field on ions based on the fact that massive ions cannot respond to the instantaneous sheath field as the mobile electrons do. With this method, the IED in collisionless rf sheaths for both low- and high-frequency regimes can be obtained and understood straightforwardly. The estimation of IEDs at high-frequency regime agrees with Benoit-Cattin's collisionless IED model according to our verification.

1.4 Dissertation Overview

This dissertation consists of three topics. The introduction is given in Chapter 1. In Chapter 2, the particle-in-cell (PIC) codes used to verify the theoretical models are briefly introduced. As two PIC codes have been used as the research progresses, a comparison of the code performance is presented.

Chapter 3 covers the IED model for a collisionless rf sheath. The collisionless sheath model is introduced. An example is shown to explain how this collisionless sheath model works. PIC simulations are run to verify the sheath model. By combining the sheath model with Benoit-Cattin's collisionless IED model, a fast computational process of predicting the IED from the initial control parameters is given and verified by PIC simulations.

In Chapter 4, a collisional sheath model with energy dependent ion mean free path λ_i is developed, as an updated alternative of the model with constant λ_i in Ref.[22]. A factor of b is introduced to express the energy dependence of λ_i (or cross section σ), with $b = 0$ standing for the constant λ_i case. A full set of expressions and estimations for the plasma parameters for the collisional rf sheath, driven by a single frequency source is given with varying λ_i.

In Chapter 5, a collisional IED model is developed to predict the IED in a collisional rf sheath, driven by a single frequency source. Ion-neutral charge exchange collisions are taken into account in the model. The energy dependent ion mean free path, time-varying sheath voltage and the oscillation motion of sheath width is considered. PIC simulations are used to verify the collisional sheath model and the IED model.

Finally, Chapter 6 gives the conclusions and suggestions for future work. Theoretical models are needed to estimate NEDs and NADs.

Chapter 2

Simulation Models

The simulations are based on planar one dimensional particle-in-cell (PIC) codes XPDP1 [42] and OOPD1, with Monte-Carlo collision methods. XPDP1 is available from University of California at Berkeley Plasma Theory and Simulation Group (PTSG) web site at http://ptsg.eecs.berkeley.edu. OOPD1 is not released to the public yet.

A flow schematic for the PIC scheme is shown in Fig. 2.1[41]. Starting from initial conditions, particle and field values are advanced sequentially in time. The particle equations of motion are advanced one time step, using fields interpolated from the discrete grid to the continuous particle locations. Next, particle boundary conditions such as absorption are applied. The Monte Carlo collision (MCC) scheme is applied for electron-neutral collisions [39]. Source terms, charge density ρ and current density J for the field equations are accumulated from the continuous particle locations to the discrete mesh locations. The fields are then advanced one time step, and the time step loop starts over again. For more information about PIC simulations, please go to Ref. [41].

The cell size $\triangle x$, and time step $\triangle t$, must be determined from Debye length λ_D, and the plasma frequency ω_p, respectively, for accuracy and stability: $\triangle x < \lambda_D = (\epsilon_0 T_e/en)^{1/2}$ and $(\triangle t)^{-1} \gg \omega_p = (e^2 n/\epsilon_0 m)^{1/2}$. Here ϵ_0 is the permitivity of free space, e is the elementary charge, and m is the mass of the lightest species (electrons). Violation of these conditions will result in inaccurate and possibly unstable solutions.

In this dissertation, XPDP1 is used to simulate the collisionless sheath, and OOPD1 is used to simulate the collisional sheath. The choice of the codes is simply based on their availability as the models are being developed. Both codes are electrostatic, having one spatial dimension, three velocity components (1d3v), and provide a self-consistent, fully kinetic representation of general plasmas. Both codes run on Unix workstations with X-Windows, and PC's with an X-Windows emulator. The PIC method enables the codes to employ the fundamental equations without much approximation, with a statistical representation of general distribution functions in phase space. Therefore, most of the physics is retained, including the nonlinear effects, and space charge and other collective effects.

Although two dimensional and three dimensional PIC codes are available for use, we

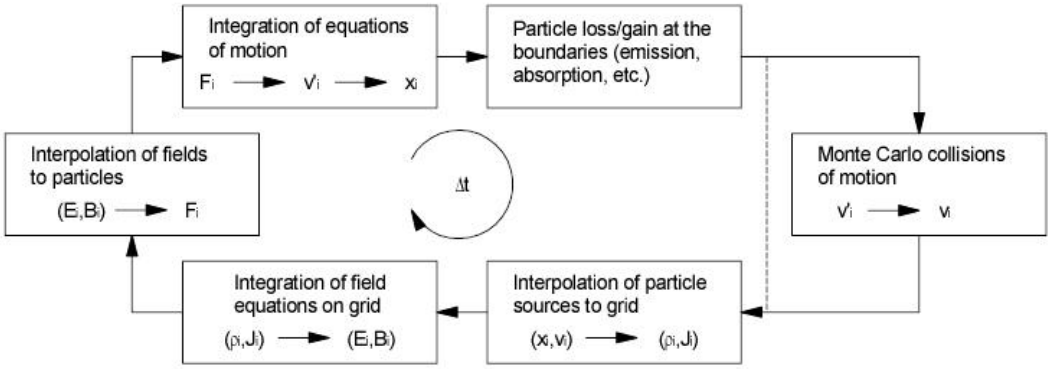

Figure 2.1: Flow schematic for the PIC scheme.

keep our research within the one dimensional domain in order to get a simple and clear understanding of the basic physics in the sheath.

2.1 XPDP1

XPDP1 is a member from the XPDx1 series family, together with XPDP1, XPDC1, XPDS1 referring to planar, cylindrical, and spherical geometries, respectively. The code compiles with standard C compilers and requires X-Windows libraries. The user specify the characteristics of the bounded plasma and the external circuit system through an input file. By specifying diagnostics at run time, the user views the output as the simulation proceeds in real-time. Code development for XPDP1 has stopped for many years.

2.2 OOPD1

OOPD1 is an object oriented plasma device one dimensional PIC code. The code compiles with standard C++ compilers. OOPD1 is considered as a more unified and extensible replacement for the previous PTSG suite of one dimensional PIC codes- the XPDx1 family. It is now being developed with powerful capability. The code is able to simulate the planar, cylindrical, and spherical coordinate systems with an improved user interface. The input file is in a more organized structure. More input parameters are able to be specified through the input file easily. It enables the control and specification of the diagnostics through the input file. During the past three years, OOPD1 has been under fast development. It has become our best choice among the PTSG PIC codes to investigate the rf sheath.

2.3 Code Comparison

The earlier work of this dissertation on the collisionless IED model was done by XPDP1. As OOPD1 is being developed with powerful capability, the later work on the collisional IED model was done by OOPD1. The motivation of switching the work from XPDP1 to OOPD1 is primarily based on the following advantages of OOPD1:

◇ Ease of switching from planar geometry to cylindrical or spherical geometries.

OOPD1 is a unified replacement for the previous PTSG suite of C 1d PIC codes: XPDP1, XPDC1, XPDS1, each of which is written for a separate coordinate system planar, cylindrical, and spherical, respectively.

◇ This allows easy switching from symmetric to asymmetric (unequal electrode areas) systems.

With a better structure of the input file and more flexibility of setting the input parameters, OOPD1 can easily deal with asymmetric systems.

◇ Ease of switching to new gas mixtures.

XPDP1 can only deal with three or fewer species. For OOPD1, users can include as many species as wanted. OOPD1 provides a clear and easy-control input structure to clarify each species in the input file. This capability enables OOPD1 to study new gas mixtures such as oxygen and argon mixed with oxygen, etc.

◇ Ease of adding fast neutral collisions, etc.

The energy and angular distribution functions of fast neutrals, NEDs and NADs are also important in plasma processing. With the flexible control of species and reactions, OOPD1 opens the door to investigating the distributions of fast neutrals on the substrate.

In a word, OOPD1 has more friendly user interface and more flexibility in applying the models to rf discharges in industry, making it a perfect tool for our studies.

2.3.1 Input file

OOPD1 has better input structure. A typical input file consists of sections of variables, species, circuit, reactions, diagnostic control, and species loading. Each species is stated clearly in the section of species with its name, charge, mass, the reaction label, and the number of physical particles per computer particle. The driving source is stated in the circuit section. The section of reactions states the reactions that the simulation considers, which provides the capability of estimating the effects of each reaction by turning on or off a specific reaction. Users can easily control the diagnostics that are of interest to observe through the diagnostic control section in the input file before the simulation starts to run. Furthermore, more advantageous than XPDP1 which can only have 3 sinusoidal rf sources, OOPD1 can simulate any driving source in any form with any number of driven sources by an arbitrary timefunction.

	XPDP1	OOPD1
No XGrafix	182.01 s	437.19 s
With XGrafix Updated Each Time Step	215.91 s	719.85 s
With XGrafix Updated Every 16 Time Steps	215.54 s	715.91 s

Table 2.1: Speed Comparison of XPDP1 and OOPD1 w/o XGrafix

2.3.2 Speed

A single frequency, voltage driven planar rf discharge in argon is simulated by XPDP1 and OOPD1 with $V_{rf} = 176$ V, $f_{rf} = 81$ MHz, $L = 0.024$ m, $A = 5.03 \times 10{-}3$ m^2, at 20 mTorr. Each case runs for 4096 time steps (4 rf periods), with 1000 cells, 10^8 physical particles per computer particle, and a time step of $1.2 \times 10{-}11$ s. It is found that XPDP1 runs 2-3 times as fast as OOPD1. The speeds of the two codes are approximately at the same level, which makes OOPD1 acceptable for further research. Details of the comparison on speed is illustrated in Table 2.1.

2.3.3 Example

The same cases are simulated by XPDP1 and OOPD1 for both single frequency and dual-frequency driven capacitive discharges, with results shown in Fig. 2.2 and Fig. 2.3, respectively. The control parameters used are: $V_{rf} = 176$ V, $f_{rf} = 81$ MHz, $L = 2.4$ cm, $A = 50.3$ cm^2, $p = 20$ mTorr for the single frequency case; $V_h = 400$ V, $f_h = 64$ MHz, $V_l = 800$ V, $f_l = 2$ MHz, $L = 3$ cm, $A = 0.5$ m^2, $p = 30$ mTorr for the dual-frequency case, with h and l in the subscripts referring to high frequency and low frequency, respectively. It is shown that OOPD1 gives the same accuracy of IEDs as XPDP1 in both cases.

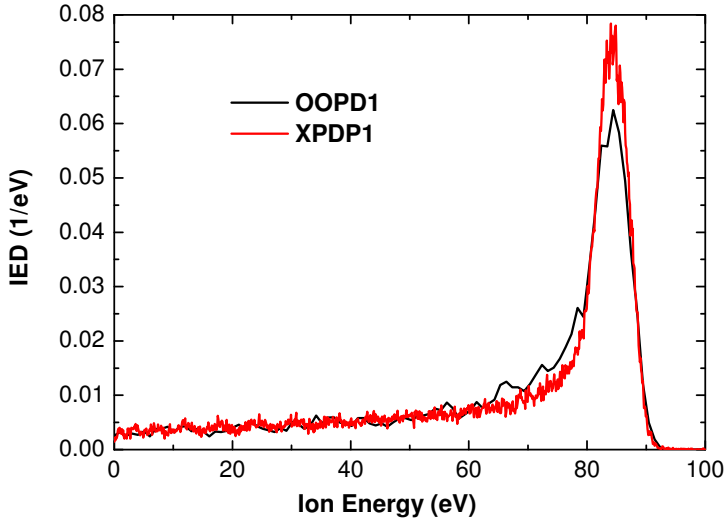

Figure 2.2: IEDs from XPDP1 and OOPD1 for a single frequency driven capacitive discharge

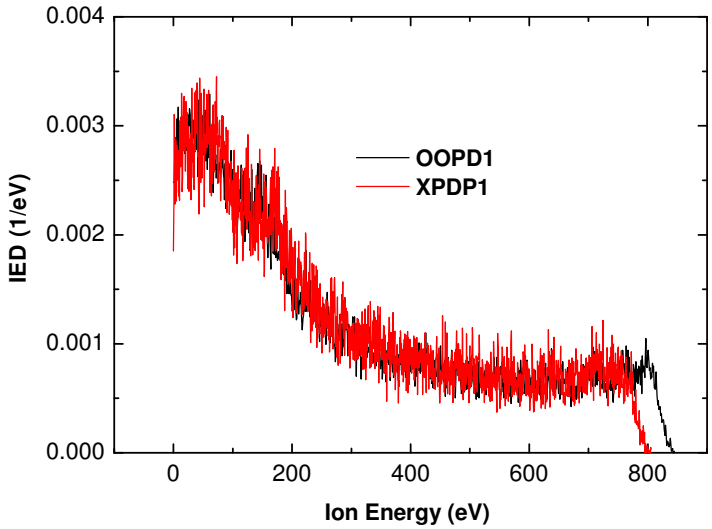

Figure 2.3: IEDs from XPDP1 and OOPD1 for a dual-frequency driven capacitive discharge

Chapter 3

Model of Collisionless Ion Energy Distributions

3.1 Introduction

For decades, considerable effects have been made to accurately control the IEDs at the substrates in capacitive discharges. However, most studies of IEDs rely on numerical methods due to the complexity of rf sheath dynamics. A fast way of predicting the IEDs is required and a simple analytical model is desired to help understand the dynamics in the rf sheath. In some commercial applications, capacitive rf discharges are operated at high density and low pressure in which the ion mean free path is much larger than the sheath width; therefore, the ion motion in the sheath can be considered collisionless. The collisionless sheath discharge model in Ref.[22] starts with the control parameters. The model gives a good estimation of the plasma parameters such as plasma density, electron temperature, dissipated power, and average ion bombarding energy. By combining this model with Benoit-Cattin's collisionless IED model in Ref. [2], which can predict the IEDs analytically with some plasma parameters specified, we have developed a method consisting of a series of simple computational steps that result in accurate IEDs for collisionless rf sheaths given the control parameters. PIC simulations are used to verify our model. Section 3.2 describes the analytical model for high voltage rf capacitive discharges in collisionless sheaths. Section 3.3 briefly explain how Benoit-Cattin's model is used in our collisionless sheath discharge model. In Section 3.4, a voltage-driven case is given as an example to show how to use this global model to obtain the plasma parameters and the IED on the substrate from the control parameters. A brief description of PIC simulations is given in section 3.5. In section 3.6, we compare the results of PIC simulations with our analytical model. Discussions and conclusions are presented. A brief summary is given in the final section.

3.2 Collisionless Sheath Model

In 1988, a simple self-consistent analytical model of collisionless rf sheath was developed [21]. Given the control parameters of the capacitive rf discharge, this model obtains expressions for the time-average ion and electron densities, electric field, and potential within the sheath. The nonlinear oscillation motion of the electron sheath boundary and the nonlinear oscillating sheath voltage is also obtained. The solution is given under the assumptions as follows: (1) The ion motion within the sheath is collisionless; the ions only respond to the time-average electric field. (2) The electrons are inertialess and respond to the instantaneous electric field; the electron sheath oscillates between a maximum thickness of s_m and a minimum thickness of a few Debye lengths from the electrode surfaces. More details are described in Ref. [23].

3.3 Collisionless IED Model

A detailed evaluation of the ion energy distributions (IEDs) can be obtained by employing an analytical model developed by Benoit-Cattin and Bernard [2]. In the model, they assume a constant sheath width $\bar{s}$, a sinusoidal sheath voltage $V_s(t) = \overline{V}_s + \widetilde{V}_s \sin\omega t$, zero initial ion velocity at the plasma-sheath boundary, and a Child-Langmuir space-charge sheath electric field. The model is valid in the high-frequency regime ($\tau_{ion}/\tau_{rf} \gg 1$), where the ions mainly respond to the time-averaged , instead of the instantaneous sheath voltage. Here $\tau_{rf} = 2\pi/\omega$ is the rf period, and τ_{ion} is the time an ion takes to traverse the sheath, which can be estimated as $\tau_{ion} = 3\bar{s}/(2e\overline{V}_s/M)^{1/2}$. The expressions for the IED $f(E)$ and the energy spread $\triangle E_i$ are

$$f(E) = \frac{dn}{dE} = \frac{2n_t}{\omega \triangle E_i}\left[1 - \frac{4}{(\triangle E_i)^2}\left(E - e\overline{V}_s\right)^2\right]^{-1/2} \tag{3.1}$$

and

$$\triangle E_i = \frac{2e\widetilde{V}_s}{\omega\bar{s}}\left(\frac{2e\overline{V}_s}{M}\right)^{1/2} = \frac{3e\widetilde{V}_s}{\pi}\left(\frac{\tau_{rf}}{\tau_{ion}}\right) \tag{3.2}$$

where n_t is the number of ions entering the sheath per unit time.

3.4 Example

We take a simple case to illustrate how the volume-averaged particle and energy balances for the collisionless sheath model works. We examine a capacitive discharge driven by a voltage source $V(t) = V_{rf}\cos(2\pi ft)$ under pressure p in argon, with f the driving frequency, $\omega = 2\pi f$ the circular frequency, L the distance between electrodes, and A the area of the electrodes. The input parameters are: $V_{rf} = 500$ V, $f = 13.56$ MHz, $p = 3$ mTorr, $l = 0.1$ m, and $A = 0.1$ m^2.

Start with an estimate of the ion sheath thickness $s_m \approx 0.01$ m, which is obtained from simulations and is a nominal value for low-pressure capacitive discharges. Using $\lambda_i = 1/330p$ (p in Torr, λ_i in cm) at 300K, the ion mean free path in the sheath is $\lambda_i = 0.01$ m. The bulk plasma length, including the presheath regions, $d \approx l - 2s_m = 0.08$ m, and $\lambda_i/d = 0.125$, which is in the intermediate mean free path regime, in which the plasma density is relatively flat in the center. The ratio between the edge density n_s and center density n_0 is given by [23]

$$h_l \equiv \frac{n_s}{n_0} \approx 0.86 \left(3 + \frac{d}{2\lambda_i}\right)^{-1/2} \tag{3.3}$$

which gives $n_s/n_0 = 0.325$. It is assumed that all the particles entering the sheath are lost to the wall. We determine the electron temperature T_e from particle balance by equating the total surface particle loss to the total volume ionization and obtain a relation as follows:

$$2n_s u_B(T_e) = K_{iz}(T_e) n_0 n_g d \tag{3.4}$$

with n_g the gas density. The explicit T_e dependences of the ionization rate constant K_{iz} and the Bohm ion loss velocity $u_B = (eT_e/M)^{1/2}$ are assumed known. A Maxwellian electron energy distribution function (EEDF) is assumed in order to calculate the rate constant based on the measured cross sections in Ref. [39]. Solving Eq. (3.4) yields $T_e \approx 3.3$ V and $u_B \approx 2.8 \times 10^3$ m/s. The collisional energy loss per electron-ion pair created, ε_c, which is T_e dependent as well, is also obtained: $\varepsilon_c \approx 64$ V [13].

Adding to this the kinetic energy loss per electron lost from the plasma with $\varepsilon_e' \approx 7.2T_e$, we get $\varepsilon_c + \varepsilon_e' \approx 88$ V. The electron-neutral collision frequency is $\nu_m \approx K_{el} n_g \approx 1.4 \times 10^7$ s^{-1}, with K_{el} given by the electron-neutral elastic scattering rate coefficient. Then the electron ohmic heating power per unit area can be determined as [23]

$$\overline{S}_{ohm} \approx 2.8 \times 10^{-17} \omega^2 V_1^{1/2} \text{ [W/m}^2\text{]} \tag{3.5}$$

where V_1 is the fundamental rf voltage amplitude across a single sheath.

For the stochastic heating power per unit area of a single sheath, we similarly obtain

$$\overline{S}_{stoc} \approx 1.6 \times 10^{-17} \omega^2 V_1 \text{ [W/m}^2\text{]} \tag{3.6}$$

As the voltage drop across the bulk plasma is relatively small at low pressures, we let $V_1 \approx V_{ab1}/2$, where V_{ab1} is the fundamental rf voltage amplitude applied to the electrodes. In our case, $V_{ab1} = 500$ V and therefore $V_1 \approx 250$ V. The time-averaged sheath voltage $\overline{V}$, which is also the ion kinetic energy per ion hitting the electrode, ε_i, is given by [23]

$$\varepsilon_i = \overline{V} \approx 0.83 V_1 \tag{3.7}$$

Then we have $\overline{V} \approx 207.5$ V.

If the system is driven by a sinusoidal current source, the roles of current and voltage sources can be switched according to the capacitive sheath relation [23]

$$J_1 \approx 1.23\frac{\omega\epsilon_0}{s_m}V_1 \tag{3.8}$$

where J_1 is the fundamental component of the current density.

The total power absorbed per unit area is found as [23]

$$S_{abs} = 2en_s u_B(\overline{V} + \varepsilon_c + \varepsilon_e') \tag{3.9}$$

From the electron power balance equation

$$S_e = \overline{S}_{ohm} + 2\overline{S}_{stoc} = 2en_s u_B(\varepsilon_c + \varepsilon_e') \tag{3.10}$$

where $\overline{S}_{ohm} + 2\overline{S}_{stoc}$ is the electron power absorbed per unit area, we get

$$S_{abs} \approx \left(\overline{S}_{ohm} + 2\overline{S}_{stoc}\right)\left(1 + \frac{\varepsilon_i}{\varepsilon_c + \varepsilon_e'}\right) \tag{3.11}$$

Substituting the value of V_1 to the expressions of $\overline{S}_{ohm}$ and $\overline{S}_{stoc}$, we find for this example that $\overline{S}_{ohm} \approx 3.25$ W/m^2 and $\overline{S}_{stoc} \approx 31.2$ W/m^2. Therefore, $S_{abs} \approx 220$ W/m^2.

From the electron power balance equation, we get $n_s \approx 8.3 \times 10^{14}$ m^{-3}. Since $n_s/n_0 \approx 0.325$, we have $n_0 \approx 2.5 \times 10^{15}$ m^{-3}.

The ion current density is obtained from the Bohm flux at the plasma sheath edge where $n_i = n_s$ from the Child law for the rf sheath,

$$\overline{J_i} = en_s u_B = K_i\epsilon_0\left(\frac{2e}{M}\right)^{1/2}\frac{\overline{V}^{3/2}}{s_m^2} \tag{3.12}$$

where $K_i = 200/243 \approx 0.82$. We get $\overline{J_i} \approx 0.38$ A/m^2 and $s_m \approx 0.0113$ m, which agrees with our initial estimate of the sheath width.

This example here has clearly shown that the collisionless sheath model is an analytical and self-consistent global model. Table 3.1 shows a set of theoretical parameters for different cases with $p = 3$ mTorr, $L = 0.1$ m, and $A = 0.1$ m^2. In the first four rows, the voltage source amplitude of 500 V is fixed and the rf frequency is varied from 6.78, 13.56, 27.12, and 40 MHz, respectively. In the fifth and sixth rows, the voltage source amplitude is shifted by $\pm 10\%$ based on the case in the second row. The last three rows present the current-driven cases at 13.56 MHz with $I_{rf} = 2.05$ A as the benchmark and the other two shifted from the source amplitude by $\pm 10\%$.

3.5 PIC Simulation

The simulations in this chapter are performed using a one-dimensional particle-in-cell code XPDP1 [42]. Ion-neutral and neutral-neutral collisions are not considered here.

We use a time step $\triangle t = 7.2 \times 10^{-11}$ s, which gives $\triangle t \approx 0.1\omega_p^{-1}$, with ω_p the plasma frequency. We use a cell size $\triangle x = 2 \times 10^{-4}$ m with 500 cells and $L = 0.1$ m, which gives $\triangle x \approx 0.5\lambda_D$, with λ_D the Debye length. The number of particles represented by a computer particle NP2C (we use NP2C = 1e8 for most cases) needs to be adjusted so that the detailed bimodal IED can be resolved statistically (the number of particles per cell is about 200), while the simulation cost (for example: time to reach a steady state) is acceptable (two days).

3.6 Results and Discussions

A semianalytical model [45] can be employed to estimate the IED. Figure 3.1 shows the scheme of this model. Besides the control parameters from the tool measurements, this model needs the sheath response from PIC simulations. The sheath voltage $V_s(t)$ (blue dash curve in the upper figure) is collected for a few rf periods from the PIC simulation after steady state. Fourier transforming $V_s(t)$, we get $V_s(f)$ (blue dash curve in the lower figure), where f is the frequency. Applying a filter $\alpha(f)$ to $V_s(f)$ (getting the black curve in the lower figure) and doing an inverse Fourier transform, we get the voltage seen by ions $V_i(t)$ (black curve in the upper figure). In Ref. [45], the filter function was chosen to be $\alpha(f) = [(c2\pi f\tau_{ion})^q + 1]^{-1/q}$ with $c = 0.3 \times 2\pi$ and $q = 5$. Since the IED within a certain small energy interval is proportional to the total time for $V_i(t)$ to lie within that energy interval, $V_i(t)$ is converted into an IED as $f(E_i) \propto |dV_i/dt|^{-1}$. This model is capable of dealing with both single and multiple- frequency driven rf sheaths, so long as the ion transit time $\tau_{ion} \ll 1/f$.

Figures 3.2 and 3.3 show the time-averaged temperature and number density for ions (dashed line) and electrons (solid line) for $V_{rf} = 500$ V at 13.56 MHz, with other control parameters remaining the same. The averaging time is eight rf periods. A fairly Maxwellian EEDF is observed. The sheath region can be identified from the sharp drop of the number densities and the position where the time-averaged ion and electron number densities branch, suggesting the maximum position of the oscillating sheath edge, or the ion sheath width s_m. To recognize the sheath edge in simulations, the sheath edge is determined by the position at which the ratio of simultaneous electron and ion number densities reaches 0.8. This factor is a reasonable value considering the unavoidable non-physical noise caused by the simulations, which is still able to reveal the physical definition of the sheath edge, where the charge neutrality is violated. Besides, the time-averaged values obtained over thousands of rf periods have reduced the effects of simulation noise by square root of the number of times in the average. A ratio of 0.6, instead of 0.8 was also used to determine the sheath edge.

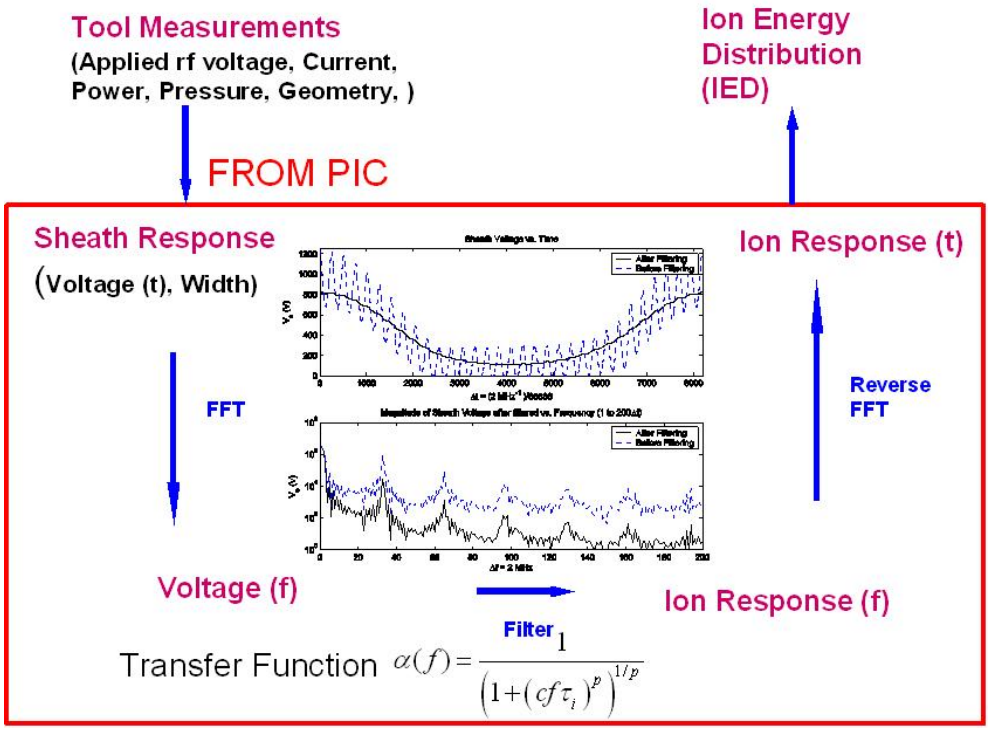

Figure 3.1: Scheme for Alan Wu's semianalytical IED model

A negligible difference, less than 5 %, in the ion sheath width was observed. The sheath width, temperatures and number densities of ions and electrons, and the ion flux found by simulations agree very well with the theoretical values of the analytical model (shown in Table 3.1).

Figure 3.4 presents the IEDs for $V_{rf} = 500$ V at 13.56 MHz, obtained from the theoretical model (solid), semianalytical model (dashed) and PIC simulation (dot-dashed). The IEDs for a current-driven case $I_{rf} = 2.05$ A are shown in Fig. 3.5. Both the semianalytical and PIC IEDs have a shift of about -20 V compared to the voltage-driven case.

To investigate the sensitivities of the current- and voltage-driven sources on the IEDs, we take the 13.56 MHz, $V_{rf} = 500$ V and $I_{rf} = 2.05$ A cases as benchmarks. We shift the sources by a $\pm 10\%$ amplitude and observe the corresponding effects the IEDs would present theoretically (shown in Fig. 3.6), and in PIC simulations (shown in Fig. 3.7). A $\pm 10\%$ shift is observed for theoretical IEDs for the voltage-driven cases (shown in Fig. 3.6 on bottom), while the current-driven cases show a larger shift, $\pm\, 12.5\%$ with the same 10% variation of the source amplitude. For the IEDs from PIC simulations, the current-driven cases also show larger shifts, $\pm\, 12\%$, given that the peak ion bombarding energy is about 20 V lower than that for the corresponding voltage-driven case.

The difference of the sensitivities of the IEDs to current or voltage sources can be well-

explained by the theoretical model, as follows: With the same shift of the source, the shift of the IED is determined by the shift of the sheath voltage V_1. For the voltage-driven discharge, $V_1 \propto V_{rf}$, the source voltage. For the current-driven discharge, with $S_{stoc} \gg S_{ohm}$, substituting Eq. (3.6) into Eq. (3.10) yields $n_s \propto V_1$. Using this in the Child law Eq. (3.12) gives $s_m \propto V_1^{1/4}$. Using this in Eq. (3.8) gives $V_1 \propto J_1^{4/3}$. Hence, a 10% shift in J_1 produces a 13.3% shift in V_1. In other words, IEDs are less sensitive to voltage-driven sources than to current-driven sources under the same conditions.

Finally, we investigate the effects of the rf frequency on the IED for a fixed rf voltage-driven source amplitude. Four cases are examined: 6.78 MHz, 13.56 MHz, 27.12 MHz, and 40 MHz. Both results from theories (shown in Fig. 3.8) and PIC simulations (shown in Fig. 3.9) show a surprising independence of the IEDs on the rf frequency. From Eq. (3.2) we can see, for a fixed source amplitude, that the ion energy spread $\triangle E_i$ is determined by the product of the sheath width s_m and the rf frequency. Varying the rf frequency changes the discharge steady states accordingly, with completely different electron temperature, number densities, etc, as shown in Table 3.1. Substituting Eq. (3.6) into Eq. (3.10) shows that $n_s \propto \omega^2$ at fixed voltage. Substituting this into the Child law Eq. (3.12) yields $s_m \propto \omega^{-1}$. Hence the product $s_m\omega$=const at fixed source voltage. Hence we find that no matter how the frequency varies, the ion energy spread given in Eq. (3.2) remains unchanged. This is seen in Table 3.1; we see that when the frequency doubles, the sheath width halves. The value of ωs_m hardly varies, which implies an unchanged IED. Equation (3.2) shows that $\triangle E_i$ is inversely proportional to τ_{ion}/τ_{rf}, which is about 2.2 for all the frequencies. For the cases we examined, the ions respond to an average sheath voltage and τ_{rf}/τ_{ion} becomes the crucial parameter in determining the shape of the IEDs. An unchanged τ_{ion}/τ_{rf} results in the independence of IEDs on the rf frequencies.

To sum up, the model provides full calculations of inside-plasma parameters including the mean ion bombarding energy with the external control factors (pressure, discharge length, rf voltage or current, and frequency) given.

3.7 Summary

A global model for high voltage rf capacitive discharges in the collisionless sheath regime is developed. Our model requires only specification of the control parameters, not relying on intermediate parameters from simulations or experimental measurement. Convincingly verified by PIC simulations, this model is able to rapidly predict the plasma parameters and the IEDs. It is a good tool for in-depth understanding of the basic physics of capacitive discharges in the collisionless sheath regime. It is found that for the same variations of rf source amplitudes, larger voltage shifts are expected in the IEDs for current-driven than voltage-driven cases. We also find that for a fixed rf voltage-driven source amplitude, the IEDs show a surprising independence on the rf frequencies. Our model gives a fast way of exploring the physics of these plasma processing discharges. The capability of verifying the

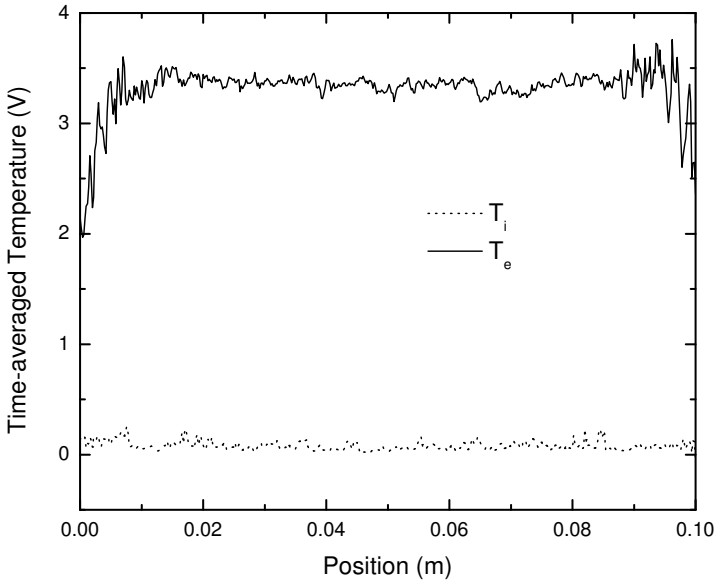

Figure 3.2: PIC time-averaged temperatures for $V_{rf} = 500V$ at 13.56 MHz

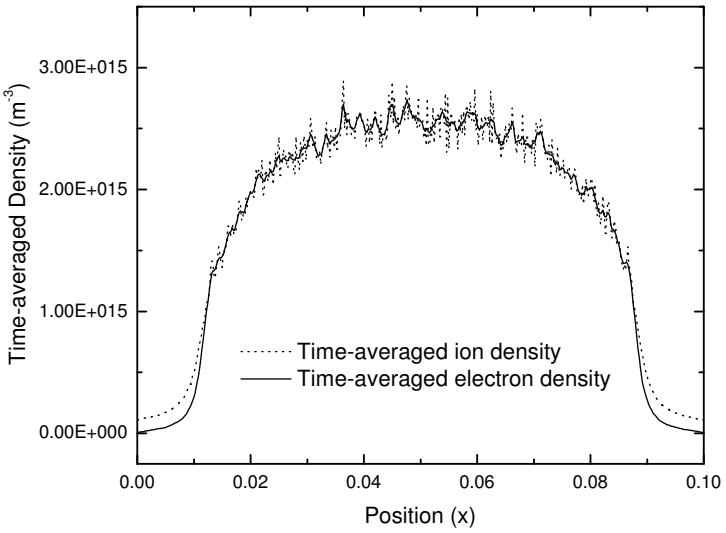

Figure 3.3: PIC time-averaged densities for $V_{rf} = 500V$ at 13.56 MHz

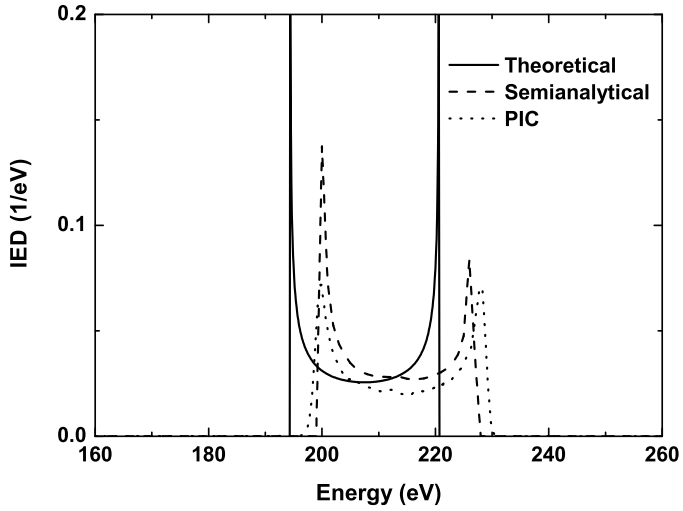

Figure 3.4: Theoretical, semianalytical, and PIC IEDs for $V_{rf} = 500V$ at 13.56 MHz

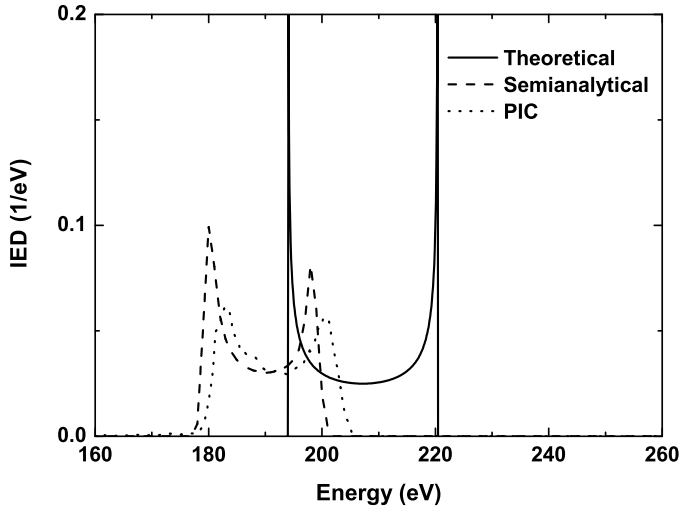

Figure 3.5: Theoretical, semianalytical, and PIC IEDs for $I_{rf} = 2.05A$ at 13.56 MHz

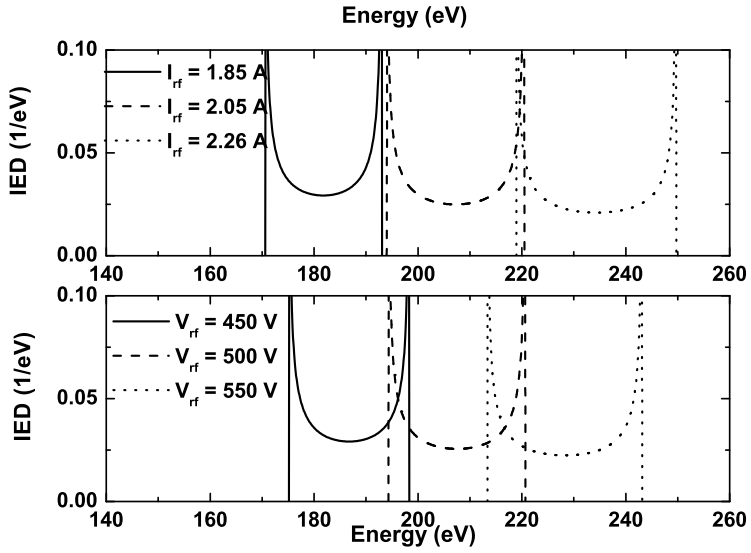

Figure 3.6: Theoretical IEDs for current-driven (top) and voltage-driven (bottom) discharges at 13.56 MHz

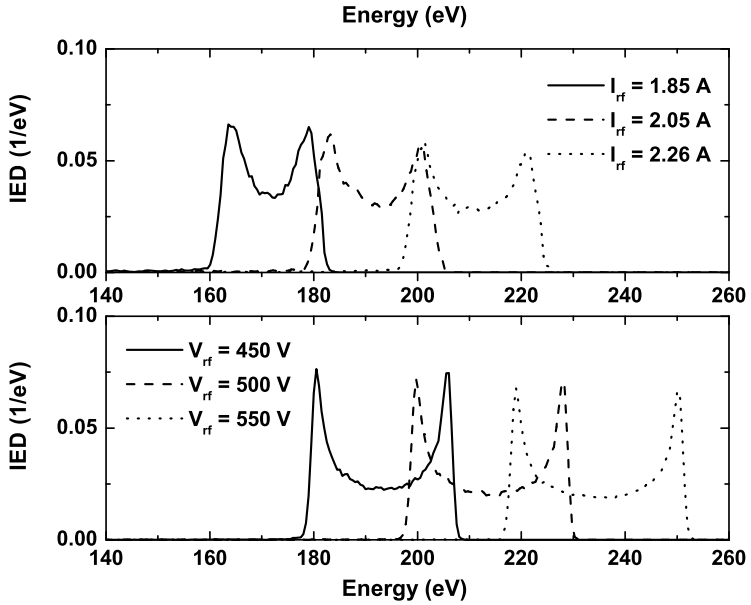

Figure 3.7: PIC IEDs for current-driven (top) and voltage-driven (bottom) discharges at 13.56 MHz

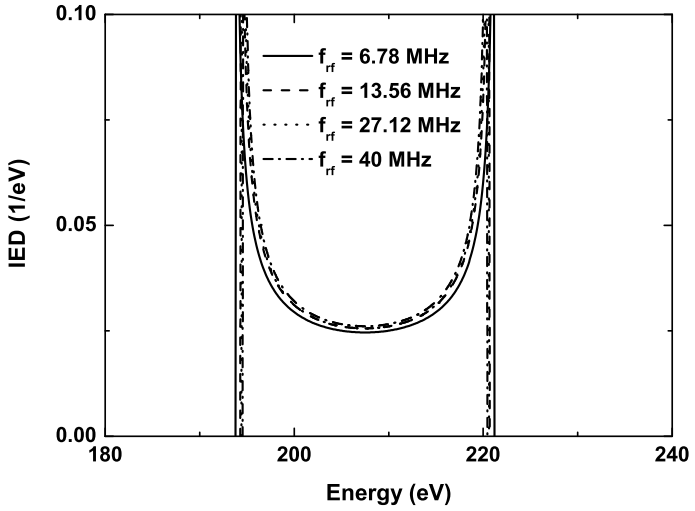

Figure 3.8: Theoretical IEDs for $V_{rf} = 500V$ at 6.78, 13.56, 27.12, and 40 MHz, respectively

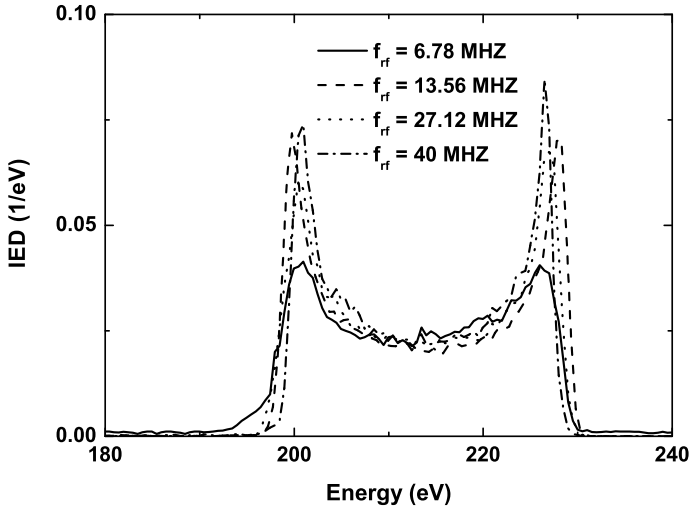

Figure 3.9: PIC IEDs for $V_{rf} = 500V$ at 6.78, 13.56, 27.12, and 40 MHz, respectively

model by PIC simulations on a highly accurate level suggests that the model can be extended to investigate multifrequency capacitive discharges, the collisional sheath regime, and other interesting topics in plasma processing.

Table 3.1: Theoretical and Simulation Discharge Parameters

V_{rf}, I_{rf}	f	T_e	T_{ePIC}	ε_c	s_m	n_0	n_{0PIC}	n_s	Γ	Γ_{PIC}	ε_i	$\triangle E_i$
500 V	6.78	3.57	3.56	59	0.0218	6.0E14	6.12E14	2.14E14	6.28E17	6.39E17	208	27.4
500 V	13.56	3.31	3.30	64	0.0113	2.52E15	2.56E15	8.30E14	2.34E18	2.39E18	208	26.4
500 V	27.12	3.20	3.16	67	0.0057	1.03E16	1.06E16	3.26E15	9.05E18	9.17E18	208	26.2
500 V	40	3.17	3.14	67	0.0036	2.25E16	2.30E16	7.05E15	1.95E19	1.98E19	208	25.9
450 V	13.56	3.30	3.30	64	0.0110	2.28E15	2.30E15	7.48E14	2.11E18	2.15E18	187	23.2
550 V	13.56	3.31	3.30	64	0.0116	2.76E15	2.82E15	9.11E14	2.57E18	2.62E18	228	29.8
1.85 A	13.56	3.30	3.23	64	0.0110	2.22E15	2.30E15	7.28E14	2.05E18	2.09E18	182	22.4
2.05 A	13.56	3.31	3.24	64	0.0113	2.52E15	2.60E15	8.30E14	2.34E18	2.39E18	207	26.4
2.26 A	13.56	3.31	3.24	64	0.0116	2.83E15	2.93E15	9.34E14	2.64E18	2.69E18	234	30.8

V_{rf}, I_{rf} - source in V, A; f - rf frequency in MHz; T_e - electron temperature in V; ε_c - collisional energy loss per electron-ion pair created in V; s_m - sheath width in m; n_0 - number density at the center in m^{-3}; n_s - number density at the sheath edge in m^{-3}; Γ - ion flux in the sheath in $m^{-2}s^{-1}$; ε_i - ion energy hitting the electrode in V; $\triangle E_i$ - ion energy spread in V; PIC in the subscript denotes the discharge parameters by simulations.

Chapter 4

Collisional Sheath Model with Energy Dependent λ_i

4.1 Introduction

In most of the existing collisional sheath models, the ion mean free path λ_i is a constant. For a typical capacitive rf discharge, the energy that ions pick up as they traverse across the sheath can range from zero to hundreds of volts. The cross section, or the collisional probability of the ion-neutral charge exchange reactions highly differs with such a wide energy range of ions. It is necessary to take into account the energy dependence of λ_i in order to achieve accurate estimation of the plasma parameters within the sheath. The work in this chapter is based on Lieberman's collisional sheath model[22], with an energy dependent ion mean free path in the form of $\lambda_i = \lambda_0(v_i/v_0)^b$. Here, λ_0 is defined as the ion mean free path at a reference velocity v_0. This updated collisional sheath model gives an analytical, self-consistent solution for a collisional sheath driven by a sinusoidal, RF current source. The basic equations and derivations are presented in Section 4.2. The effective sheath capacitance and conductance is determined in Section 4.3 and 4.4. We give an example in Section 4.5, showing some important plasma parameters for varying energy dependence of the ion mean free path. By setting the factor of b to zero, the model can reproduce the results in Ref.[22]. A brief summary is given in the final section.

4.2 Basic Equations

The derivations are based on Ref.[21, 22]. The Maxwell equation for the instantaneous electric field $E(x,t)$ within the sheath is

$$\begin{aligned} \frac{\partial E}{\partial x} &= \frac{e}{\epsilon_0} n_i(x), \quad s(t) < x \\ &= 0, \quad s(t) > x. \end{aligned} \tag{4.1}$$

Here, s(t) is the distance from the ion-sheath boundary at $x = 0$ to the electron-sheath edge. ϕ is defined as: $s(t) = x$ for $\omega t = \pm\phi$.

The equations for the time-average electric field $\bar{E}(x)$ and potential $\bar{\Phi}(x)$ are:

$$\frac{d\bar{E}}{dx} = \frac{e}{\epsilon_0}(n_i(x) - \bar{n}_e(x)) \tag{4.2}$$

$$\frac{d\bar{\Phi}}{dx} = -\bar{E} \tag{4.3}$$

The equation for the electron-sheath motion is obtained by equating the displacement current to the conduction current at the electron-sheath edge:

$$-en_i(s)\frac{ds}{dt} = -\tilde{J}_0 \sin\omega t \tag{4.4}$$

We integrate Eq. 4.1 to obtain

$$\begin{aligned} E &= \frac{e}{\epsilon_0}\int_s^x n_i(\zeta)d\zeta, \quad s(t) < x \\ &= 0, \quad s(t) > x. \end{aligned} \tag{4.5}$$

We integrate Eq. 4.4 to obtain

$$\frac{e}{\epsilon_0}\int_0^s n_i(\zeta)d\zeta = \frac{\tilde{J}_0}{\epsilon_0\omega}(1 - \cos\omega t) \tag{4.6}$$

where we have chosen the integration constant so that $s(t) = 0$ at $\omega t = 0$. From Eq. 4.5 and Eq. 4.6 we obtain

$$\begin{aligned} E(x,\omega t) &= \frac{e}{\epsilon_0}\int_0^x n_i(\zeta)d\zeta - \frac{\tilde{J}_0}{\epsilon_0\omega}(1 - \cos\omega t), \quad s(t) < x \\ &= 0, \quad s(t) > x. \end{aligned} \tag{4.7}$$

Inserting Eq. 4.6 with $s = x$, $\omega t = \phi$ into Eq. 4.7 we obtain the instantaneous and time-average electric fields:

$$\begin{aligned} E(x,\omega t) &= \frac{\tilde{J}_0}{\epsilon_0\omega}(\cos\omega t - \cos\phi), \quad s(t) < x \\ &= 0, \quad s(t) > x. \end{aligned} \tag{4.8}$$

and

$$\bar{E} = \frac{\tilde{J}_0}{\epsilon_0\omega\pi}(\sin\phi - \phi\cos\phi) \tag{4.9}$$

The ion particle conservation equation is,

$$n_i v_i = n_0 u_B \tag{4.10}$$

The ion momentum conservation equations for collisionless and collisional rf sheaths are, respectively,

$$\frac{1}{2} M v_i^2 = \frac{1}{2} u_B^2 - e\bar{\Phi} \tag{4.11}$$

$$v_i = \mu_i \bar{E} = \frac{2e\lambda_i}{\pi M v_i} \bar{E} \tag{4.12}$$

Here, μ_i is the mobility and $\bar{E}$ is the time-averaged electric field. By assuming $\lambda_i = \lambda_0 (v_i/v_0)^b$, with λ_0 the ion mean free path at reference ion velocity v_0 at ion temperature $T_i = 0.05\ V$, we have Eq. 4.12 modified for the energy dependent λ_i as follows:

$$v_i = \frac{2e\lambda_0 \left(\frac{v_i}{v_0}\right)^b}{\pi M v_i} \bar{E} \tag{4.13}$$

Therefore, we have

$$v_i^{2-b} = \frac{2e\lambda_0 v_0^{-b}}{\pi M} \bar{E} \tag{4.14}$$

By substituting v_i in Eq. 4.10 with the above expression, we get

$$n_i = n_0 u_B \left(\frac{2e\lambda_0 \bar{E}}{\pi M} v_0^{-b} \right)^{-\frac{1}{2-b}} \tag{4.15}$$

For a constant λ_i, $b = 0$. By setting $b = 0$ in Eq. 4.15, we obtain the same expression of n_i as in Ref.[22].

Inserting Eq. 4.15 into Eq. 4.4 with $s = x$, $\omega t = \phi$, we obtain

$$\frac{d\phi}{dx} = \frac{u_B}{\tilde{s}_0} \left(\frac{\pi M}{2e\lambda_0} \right)^{\frac{1}{2-b}} v_0^{\frac{b}{2-b}} \frac{1}{\bar{E}^{\frac{1}{2-b}} \sin\phi} \tag{4.16}$$

where

$$\tilde{s}_0 = \tilde{J}_0 / (e\omega n_0) \tag{4.17}$$

is an effective oscillation amplitude.

Again, by setting $b = 0$ in Eq. 4.16, we obtain the same expression of $d\phi/dx$ as in Ref.[22] for a constant λ_i in a collisional rf sheath.

Inserting Eq. 4.9 into Eq. 4.16 and integrating, we obtain

$$\frac{x}{\tilde{s}_0} = H \int_0^{\phi} (\sin\zeta - \zeta\cos\zeta)^{\frac{1}{2-b}} \sin\zeta d\zeta \tag{4.18}$$

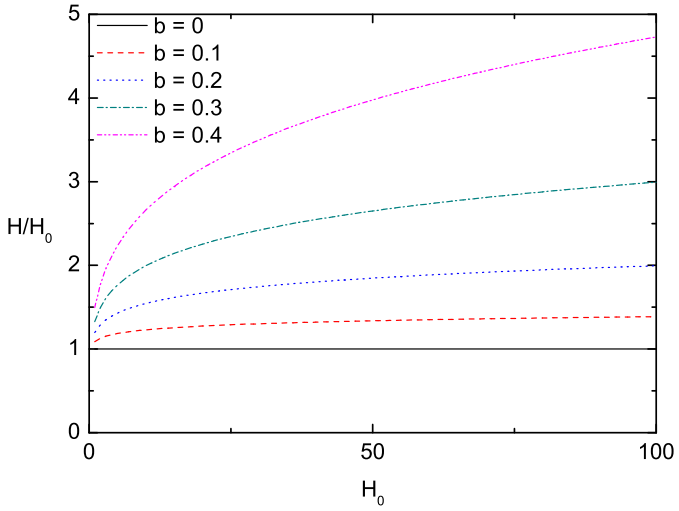

Figure 4.1: H/H_0 versus H_0 for varying b

where

$$H = \left(\frac{2\lambda_0 \tilde{s}_0}{\pi^2}\frac{e^2 n_0}{\epsilon_0 M}\right)^{\frac{1}{2-b}} v_0^{-\frac{b}{2-b}} \left(\frac{M}{eT_e}\right)^{1/2} \tag{4.19}$$

By setting $b = 0$ in Eq. 4.19, we obtain

$$H_0 = \left(\frac{2\lambda_0 \tilde{s}_0}{\pi^2 \lambda_D^2}\right)^{1/2} \tag{4.20}$$

with $\lambda_D = (\epsilon_0 T_e/en_0)^{1/2}$, the same as in Ref.[22] for a constant λ_i in a collisional rf sheath. The effects of b on the value of H are shown in Fig. 4.1. As we will see from the later derivation, H is a factor that appears in almost all the expressions of the important plasma parameters. The discrepancy of H (the energy dependent λ_i case) from H_0 (the constant λ_i case) gets larger as the value of H_0 increases. It is also shown very clearly in Fig. 4.2 that this discrepancy increases with b. Therefore, for the collisional rf discharges with a high H_0, it is required to consider the energy dependence of λ_i. Making the simplifying assumption of a constant λ_i would achieve inaccurate results.

Comparing Eq. 4.19 with Eq. 4.20, we get

$$H = H_0^{\frac{2}{2-b}} \left(\frac{u_B}{v_0}\right)^{\frac{b}{2-b}} \tag{4.21}$$

Setting $x = s(t)$ and $\phi = \omega t$ in Eq. 4.18, we obtain the nonlinear oscillation motion of the electron sheath, which is shown in Fig. 4.3 with x normalized by H (top) and H_0

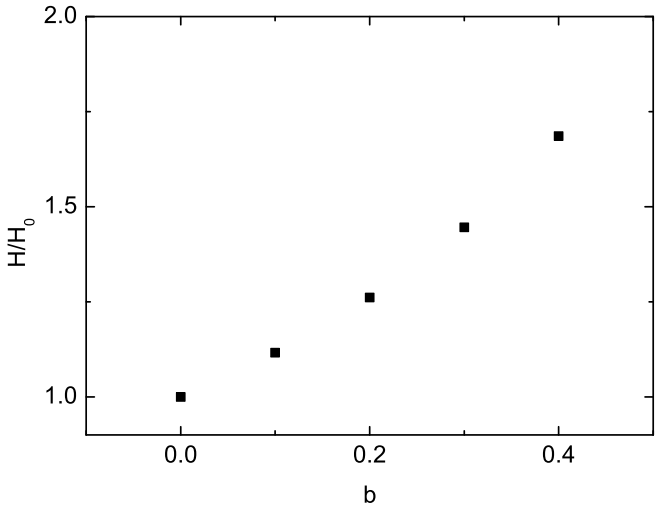

Figure 4.2: H/H_0 versus b

(bottom), respectively. As we can see from Eq. 4.18, H behaves the same for the energy dependent λ_i case as H_0 does for the constant λ_i case in Ref.[22]. The effects of b on x come from two parts: H and the integrand (b in the exponent). The top plot with x normalized by H shows that the effects of b in the integrand is very small. This implies that, by only updating the value of H from the constant λ_i case while keeping the integrand (also b affected) remaining unchanged in Eq. 4.18, it is convenient and appropriate to obtain x for the energy dependent λ_i case from the constant λ_i case. From the bottom plot in Fig. 4.3 we can also see the necessity of considering λ_i as an energy dependent function.

Setting $s = s_m$ at $\phi = \pi$ in Eq. 4.18, we obtain the ion-sheath thickness as a function of b numerically. Define the coefficients C_{sm} and C'_{sm}: $s_m = C_{sm}H_0\tilde{s}_0 = C'_{sm}H\tilde{s}_0$, with $C_{sm} = C'_{sm} = C_{sm0}$ for $b = 0$. The normalized C_{sm} (bottom) and C'_{sm} (top) for varying b are shown in Fig. 4.4. The ion-sheath thickness in the collisional sheaths for an energy dependent λ_i is listed in Eq. 4.22 for various b values, with $b = 0$ representing the case for a constant λ_i [22].

$$\begin{aligned} s_m &= 1.92H_0\tilde{s}_0 = 1.92H\tilde{s}_0, \quad b = 0 \\ &= 2.16H_0\tilde{s}_0 = 1.93H\tilde{s}_0, \quad b = 0.1 \\ &= 2.46H_0\tilde{s}_0 = 1.95H\tilde{s}_0, \quad b = 0.2 \\ &= 2.84H_0\tilde{s}_0 = 1.97H\tilde{s}_0, \quad b = 0.3 \\ &= 3.35H_0\tilde{s}_0 = 1.99H\tilde{s}_0, \quad b = 0.4. \end{aligned} \tag{4.22}$$

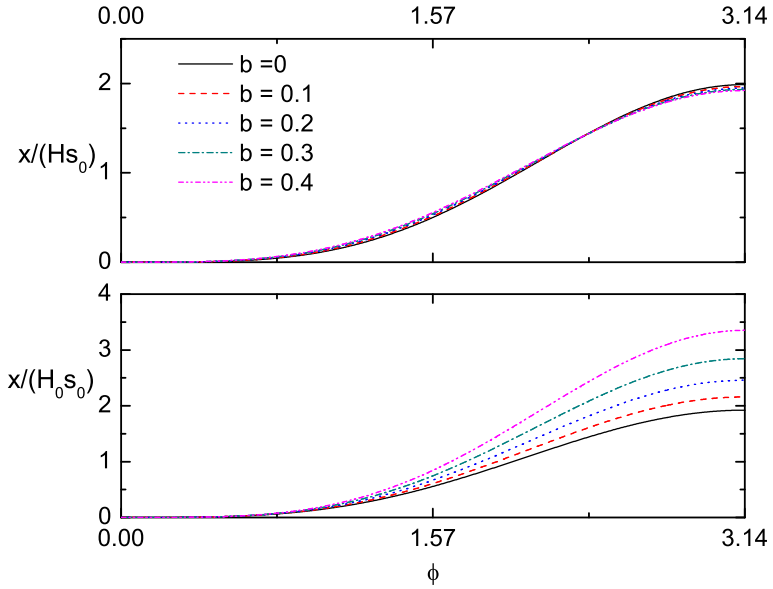

Figure 4.3: Normalized position versus phase for varying b

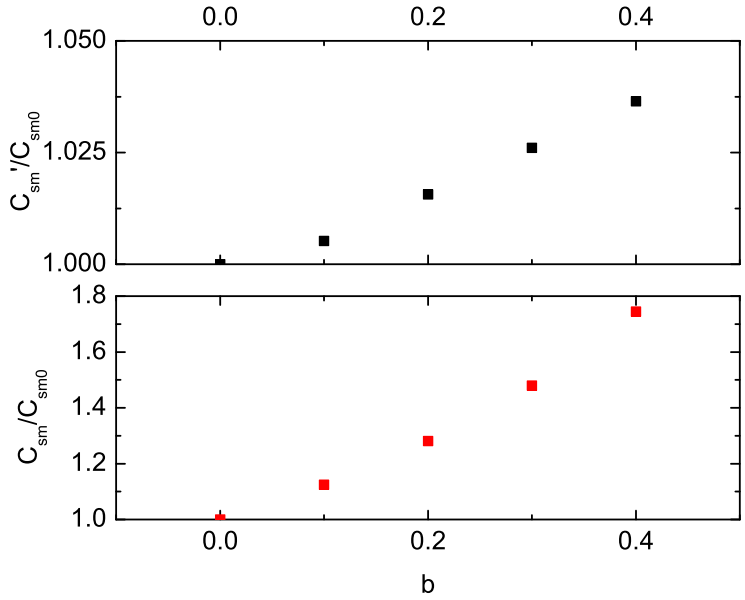

Figure 4.4: Normalized C_{sm} versus b

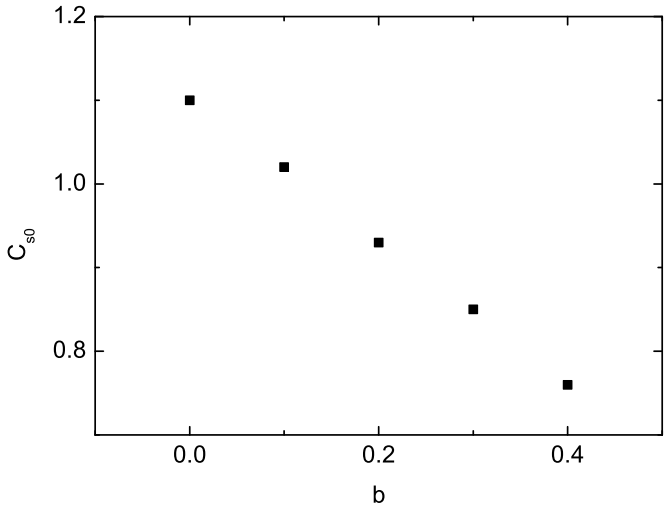

Figure 4.5: C_{s0} versus b

For a given discharge, H_0 is a constant, while H is variable, dependent on the value of b. In other words, choosing different energy dependences of ion-neutral mean free path (different b) will result in different relations of the ion-sheath thickness, which, for a self-consistent model, will result in different plasma parameters.

Substituting Eq. 4.19 in the above expression for s_m and solving for $\tilde{s}_0$, we obtain

$$\begin{aligned}
\tilde{s}_0 &= 1.10\lambda_D^{2/3} s_m^{2/3}/\lambda_0^{1/3}, \quad b = 0 \\
&= 1.02\lambda_D^{2/3} s_m^{2/3}/\lambda_0^{1/3}, \quad b = 0.1 \\
&= 0.93\lambda_D^{2/3} s_m^{2/3}/\lambda_0^{1/3}, \quad b = 0.2 \\
&= 0.85\lambda_D^{2/3} s_m^{2/3}/\lambda_0^{1/3}, \quad b = 0.3 \\
&= 0.76\lambda_D^{2/3} s_m^{2/3}/\lambda_0^{1/3}, \quad b = 0.4.
\end{aligned} \tag{4.23}$$

Define the coefficient C_{s0}: $\tilde{s}_0 = C_{s0}\lambda_D^{2/3} s_m^{2/3}/\lambda_0^{1/3}$. C_{s0} for varying b is plotted in Fig. 4.5. The time-average electric field is given by Eq. 4.9 with $\phi(x)$ obtained from Eq. 4.16. $\bar{E}$ for varying b is plotted in Fig. 4.6. The ion density $n_i(x)$ in Eq. 4.15 for varying b is plotted in Fig. 4.7.

The time-average potential is found by inserting Eq. 4.9 into Eq. 4.3 and integrating, which yields

$$\bar{\Phi} = -\frac{\tilde{J}_0}{\pi\epsilon_0\omega}\int_0^{\phi}(\sin\zeta - \zeta\cos\zeta)\frac{dx}{d\zeta}d\zeta \tag{4.24}$$

Using Eq. 4.16 along with Eq. 4.9 and Eq. 4.17 in Eq. 4.24, we obtain

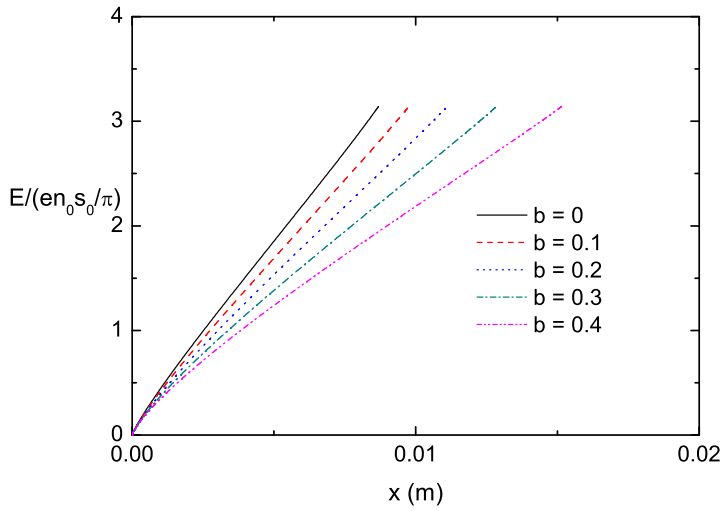

Figure 4.6: Normalized dc electric field versus position for varying b

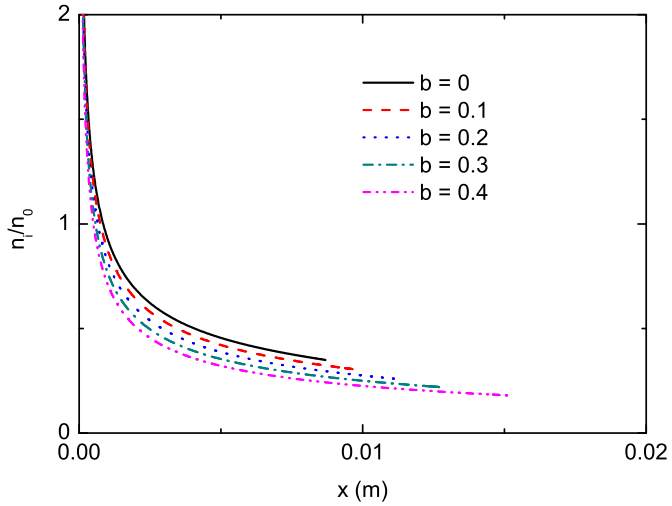

Figure 4.7: Normalized ion density n_i/n_0 versus position for varying b

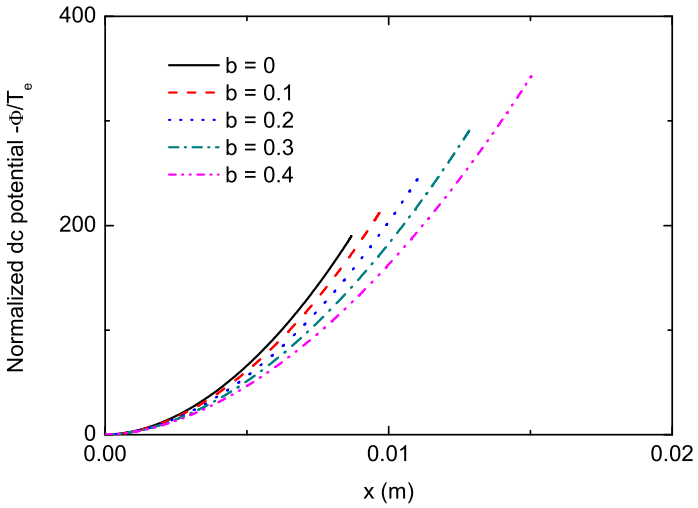

Figure 4.8: Normalized dc potential Φ/T_e versus position for varying b

$$\frac{\bar{\Phi}}{T_e} = -\frac{H}{\pi}\frac{\tilde{s}_0^2}{\lambda_D^2}\int_0^{\phi}(\sin\zeta - \zeta\cos\zeta)^{\frac{3-b}{2-b}}\sin\zeta d\zeta \tag{4.25}$$

The total dc voltage across the sheath can be obtained by setting $\phi = \pi$ and $\bar{\Phi} = -\bar{V}$ in Eq. 4.25 and evaluating the integral numerically, which is shown in Fig. 4.8.

The total dc voltage across the sheath is related to the dc ion current and the ion sheath thickness by an expression in the form of Child's law:

$$J_i = K\epsilon_0\left(\frac{2e}{M}\right)^{1/2}\frac{\bar{V}^{3/2}}{s_m^2} \tag{4.26}$$

where $J_i = en_0u_B$ is the dc ion current and $\bar{V} = -\bar{\Phi}(\phi = \pi)$ is the voltage across the sheath. Setting $\phi = \pi$ and $\bar{\Phi} = -\bar{V}$ in Eq. 4.25 and evaluating the integral numerically, we obtain $\bar{V}$ for different values of b:

$$\begin{aligned}
\frac{\bar{V}}{T_e} &= 3.15\frac{H_0}{\pi}\frac{\tilde{s}_0^2}{\lambda_D^2} = 3.15\frac{H}{\pi}\frac{\tilde{s}_0^2}{\lambda_D^2}, \quad b = 0 \\
&= 3.58\frac{H_0}{\pi}\frac{\tilde{s}_0^2}{\lambda_D^2} = 3.21\frac{H}{\pi}\frac{\tilde{s}_0^2}{\lambda_D^2}, \quad b = 0.1 \\
&= 4.12\frac{H_0}{\pi}\frac{\tilde{s}_0^2}{\lambda_D^2} = 3.27\frac{H}{\pi}\frac{\tilde{s}_0^2}{\lambda_D^2}, \quad b = 0.2
\end{aligned}$$

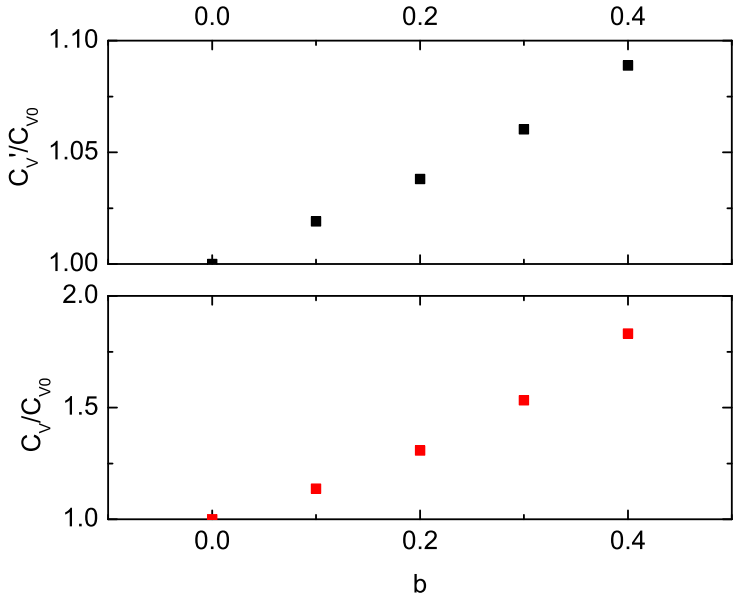

Figure 4.9: Normalized C_V versus b

$$\begin{aligned} &= 4.83\frac{H_0}{\pi}\frac{\tilde{s}_0^2}{\lambda_D^2} = 3.34\frac{H}{\pi}\frac{\tilde{s}_0^2}{\lambda_D^2}, \quad b = 0.3 \\ &= 5.77\frac{H_0}{\pi}\frac{\tilde{s}_0^2}{\lambda_D^2} = 3.43\frac{H}{\pi}\frac{\tilde{s}_0^2}{\lambda_D^2}, \quad b = 0.4. \end{aligned} \tag{4.27}$$

Define the coefficients C_V and C_V': $\frac{\bar{V}}{T_e} = C_V\frac{H_0}{\pi}\frac{\tilde{s}_0^2}{\lambda_D^2} = C_V'\frac{H}{\pi}\frac{\tilde{s}_0^2}{\lambda_D^2}$, with $C_V = C_V' = C_{V0}$ at $b = 0$. The normalized C_V and C_V' for varying b is plotted in Fig. 4.9.

Using Eq. 4.19 and Eq. 4.17 in Eq. 4.27 and the definitions for λ_D and J_i, we obtain Eq. 4.26 with

$$K = \pi^{3/2}/2^{1/2}(C_{sm}/(C_V C_{s0}))^{3/2}(\lambda_0/s_m)^{1/2} \tag{4.28}$$

For collisionless ion motion in the sheath [21], the self-consistent result is $K_f = 0.82$. For collisional ion motion with the energy dependent λ_i, we get

$$\begin{aligned} K &= 1.62(\lambda_0/s_m)^{1/2}, \quad b = 0 \\ &= 1.79(\lambda_0/s_m)^{1/2}, \quad b = 0.1 \\ &= 2.03(\lambda_0/s_m)^{1/2}, \quad b = 0.2 \\ &= 2.27(\lambda_0/s_m)^{1/2}, \quad b = 0.3 \\ &= 2.63(\lambda_0/s_m)^{1/2}, \quad b = 0.4. \end{aligned} \tag{4.29}$$

4.3 Sheath Capacitance

Integrating Eq. 4.8 with respect to x, we obtain the instantaneous voltage from the plasma to the electrode across the sheath:

$$V(t) = \int_s^{s_m} E(x,t)dx. \tag{4.30}$$

Changing variables from x to ϕ and using Eq. 4.8, we obtain

$$V(t) = \frac{\tilde{J}_0}{\epsilon_0 \omega} \int_{\omega t}^{\pi} (\cos\omega t - \cos\phi) \frac{dx}{d\phi} d\phi. \tag{4.31}$$

Using Eq. 4.9 and Eq. 4.16 to evaluate $dx/d\phi$ in Eq. 4.31 we obtain, for $0 < \omega t < \pi$,

$$V(t) = \left(en_0\tilde{s}_0^2/\epsilon_0\right) H \int_{\omega t}^{\pi} (\cos\omega t - \cos\phi)\,(\sin\phi - \phi\cos\phi)^{\frac{1}{2-b}} \sin\phi d\phi. \tag{4.32}$$

$V(t)$ is an even, periodic function of ωt with period 2π. For $-\pi < \omega t < \pi$, $V(t)$ is given by the right hand side of Eq. 4.32 with ωt replaced by $-\omega t$. Figure 4.10 shows the sheath voltage versus ωt normalized with H (top) and H_0, respectively for varying b. The peak value of $V(t)$ occurs at $\omega t = 0$:

$$\begin{aligned}
V(0) &= 2.50H_0(en_0\tilde{s}_0^2/\epsilon_0) = 2.50H(en_0\tilde{s}_0^2/\epsilon_0), \quad b = 0 \\
&= 2.83H_0(en_0\tilde{s}_0^2/\epsilon_0) = 2.54H(en_0\tilde{s}_0^2/\epsilon_0), \quad b = 0.1 \\
&= 3.25H_0(en_0\tilde{s}_0^2/\epsilon_0) = 2.58H(en_0\tilde{s}_0^2/\epsilon_0), \quad b = 0.2 \\
&= 3.80H_0(en_0\tilde{s}_0^2/\epsilon_0) = 2.63H(en_0\tilde{s}_0^2/\epsilon_0), \quad b = 0.3 \\
&= 4.52H_0(en_0\tilde{s}_0^2/\epsilon_0) = 2.68H(en_0\tilde{s}_0^2/\epsilon_0), \quad b = 0.4.
\end{aligned} \tag{4.33}$$

By setting $V(0) = C'_{Vm}H(en_0\tilde{s}_0^2/\epsilon_0) = C_{Vm}H_0(en_0\tilde{s}_0^2/\epsilon_0)$, with $C_{Vm} = C_{Vm0}$ at $b = 0$, we plot the normalized coefficient in the peak sheath voltage C'_{Vm}/C_{Vm0} and C_{Vm}/C_{Vm0} versus b in Fig. 4.11. Expanding $V(t)$ in a Fourier series

$$V(t) = \sum_{k=0}^{\infty} V_k \cos k\omega t \tag{4.34}$$

for $b = 0$, we obtain the same result as in Ref.[22]:

$$\begin{aligned}
V_0 &= \bar{V} = 1.00H(en_0\tilde{s}_0^2/\epsilon_0), \\
V_1 &= 1.28H(en_0\tilde{s}_0^2/\epsilon_0), \\
V_2 &= 0.25H(en_0\tilde{s}_0^2/\epsilon_0), \\
V_3 &= -0.034H(en_0\tilde{s}_0^2/\epsilon_0).
\end{aligned} \tag{4.35}$$

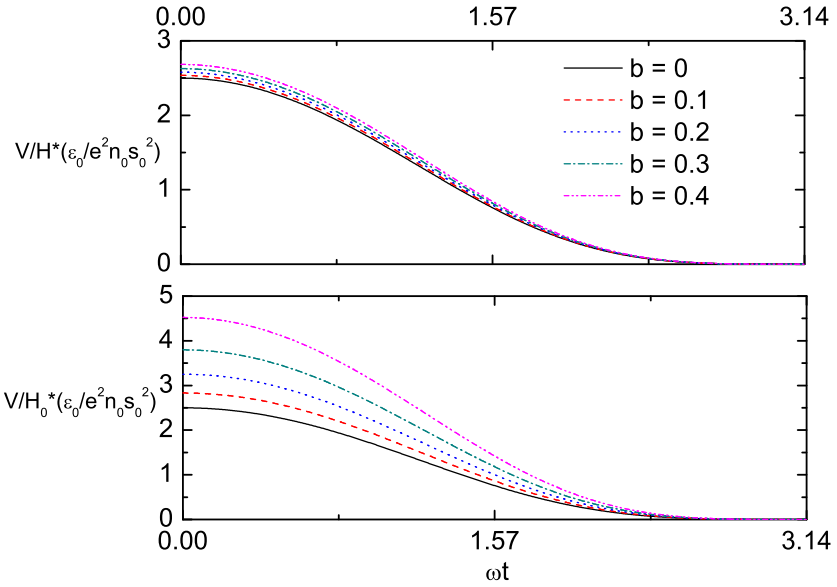

Figure 4.10: Normalized sheath voltage versus phase for varying b

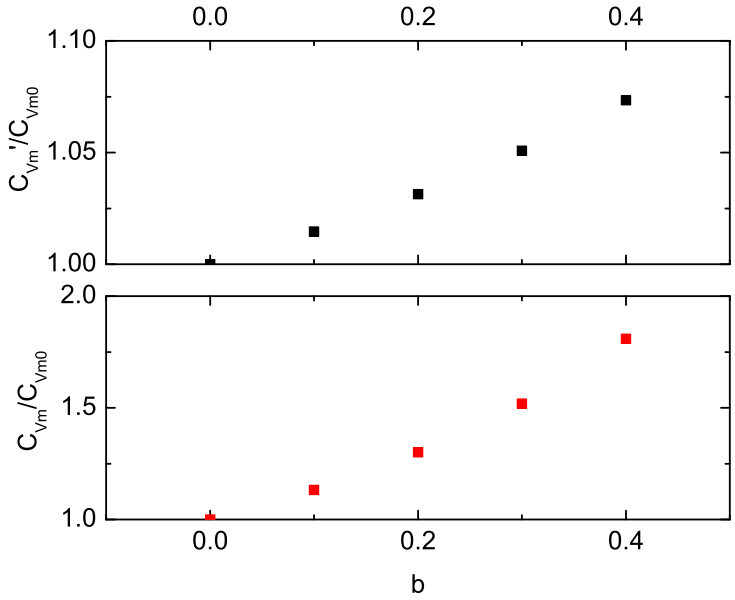

Figure 4.11: Normalized C_{Vm} versus b

Results for varying b are shown in Table 4.1.

The effective capacitance per unit area is defined from the relation

$$-\tilde{J}_0 \sin\omega t = C'_s \frac{d}{dt}(V_1 \cos\omega t) \tag{4.36}$$

. Using Eq. 4.17 along with the relation of $s_m = C'_{sm} H s_0$ and $V_1 = C'_1 H(en_0\tilde{s}_0^2/\epsilon_0)$, we get

$$C'_s = \frac{C'_{sm}}{C'_1}\frac{\epsilon_0}{s_m} \tag{4.37}$$

with $C'_s = 1.52\epsilon_0/s_m$ for $b = 0$ and $C'_s = 1.44\epsilon_0/s_m$ for $b = 0.4$. The value of the coefficient in this relation decreases as b increases. For collisionless ion motion in the sheath [21], the coefficient is 1.23.

4.4 Sheath Conductance

Follow the procedure in Ref.[22] to calculate the sheath conductance in a collisional sheath with varying b. The expression of the sheath velocity $u_s = ds/dt$ is generalized as

$$u_s = \tilde{u}_0 H(\sin\phi - \phi\cos\phi)^{1/(2-b)} \sin\phi \tag{4.38}$$

Here, $\tilde{u}_0$ is the amplitude of the oscillation velocity of the plasma electrons $u_0(t)$ at the ion-sheath edge $x = 0$, $n_s u_s = \tilde{u}_0 n_0 \sin\phi$. The dc power transferred to the electrons per unit area is given by $\bar{S} = 4m\Gamma_s n_0^{-1}\langle(u_s - u_0)u_s n_s\rangle_\phi$. Here, Γ_s is the electron-flux incident on the ion-sheath edge. For a Maxwellian distribution, $\Gamma_s = \frac{1}{4}n_0 u_e$ with $u_e = (8eT_e/\pi m)^{1/2}$ the mean electron speed. Doing the substitution in $\bar{S}$, we obtain

$$\bar{S} = Hmn_0 u_e \tilde{u}_0^2 \langle(\sin\phi - \phi\cos\phi)^{1/(2-b)} \sin\phi^2\rangle_\phi \tag{4.39}$$

Set $\bar{S} = C'_{\bar{S}} H m n_0 u_e \tilde{u}_0^2$, we get $C'_{\bar{S}}$ for varying b: $C'_{\bar{S}} = 0.491,\ 0.493,\ 0.496,\ 0.5,\ 0.503$ for $b = 0,\ 0.1,\ 0.2,\ 0.3,\ 0.4$, respectively. The effective surface conductance per unit area is defined

$$G'_s = \frac{\tilde{J}_0^2}{2\bar{S}} \tag{4.40}$$

where $\tilde{J}_0 = en_0\tilde{u}_0$.

Taking Eq. 4.39 into Eq. 4.40 we obtain

$$G'_s = \frac{1}{2C'_{\bar{S}}H}\left(\frac{e^2 n_0}{mu_e}\right) \tag{4.41}$$

Using Eq. 4.21, Eq. 4.20, and $\tilde{s}_0 = C_{s0}\lambda_D^{2/3} s_m^{2/3}/\lambda_0^{1/3}$, we obtain

$$H = \left(\frac{2C_{s0}}{\pi^2}\right)^{\frac{1}{2-b}} \left(\frac{\lambda_0 s_m}{\lambda_D^2}\right)^{\frac{2}{3(2-b)}} \left(\frac{u_B}{v_0}\right)^{\frac{b}{2-b}} \tag{4.42}$$

For $b = 0$, the coefficient $\left(\frac{2C_{s0}}{\pi^2}\right)^{\frac{1}{2-b}}$ in Eq. 4.42 is 0.47. This result agrees with the constant ion mean free path case (see Eq. 38, [22]).

Using Eq. 4.42 and Eq. 4.41 we then obtain

$$G'_s = \frac{1}{2C'_{\bar{S}}} \left(\frac{\pi^2}{2C_{s0}}\right)^{\frac{1}{2-b}} \left(\frac{v_0}{u_B}\right)^{\frac{b}{2-b}} \left(\frac{\lambda_D^2}{\lambda_0 s_m}\right)^{\frac{2}{3(2-b)}} \left(\frac{e^2 n_0}{m u_e}\right) \tag{4.43}$$

As we can see from the above derivations that, the expressions of the plasma parameters for an energy dependent λ_i case, for example, the oscillating sheath edge x and the sheath voltage V, can be updated from the constant λ_i case [22] by two procedures: modifying H using Eq. 4.21; adding the b related power to the integrand, as shown in Eq. 4.18 for the oscillating sheath motion and Eq. 4.32 for the sheath voltage. The effect of b on the modification of H is always large, as the primary b-effect carrier; while the other carrier, b in the integrand, can be negligible for some parameters (i.e., sheath motion) and preferably retained (i.e., sheath voltage).

4.5 Example

As an example, we choose $J_0 = 32$ A/m^2, $p = 40$ mTorr, $\omega = 2\pi \times 13.56\ MHz$, $T_e = 2.5$ eV, $n_0 = 8.5 \times 10^{14}$ m^{-3}, and $M = 40$ amu (i.e., argon). J_0 is the amplitude of the rf current density passing through the sheath; n_0 is the plasma density at the ion-sheath edge. Then we obtain $\lambda_D = 4.03 \times 10^{-3}$ m, $u_B = 2.44 \times 10^3$ m/s, $u_e = 1.06 \times 10^6$ m/s, $J_i = 0.33$ A/m^2, $\tilde{s}_0 = 2.76 \times 10^{-3}$ m, $v_0 = 4.89 \times 10^2$ m/s, and $\lambda_0 = 7.58 \times 10^{-4}$ m. u_e is the mean electron speed; J_i is the dc ion current; $\tilde{s}_0$ is the effective oscillation amplitude; λ_0 is the reference ion mean free path at the reference velocity v_0 (at $T_i = 0.05$ eV). For varying b, some parameters are shown in Table 4.2. As the value of b increases, λ_i within the sheath gets larger, which is more closer to a collisionless sheath case. As shown in the change of C'_s and G'_s for the increasing b, the sheath capacitance and conductance decreases.

4.6 Summary

An updated analytical, self-consistent model for collisional, capacitive RF sheaths with the energy dependent ion mean free path λ_i is developed, based on the model in Ref. [22] with a constant ion mean free path. The effects of the energy dependence of the ion mean free path are studied for various plasma parameters within the sheath. A simple method of generalizing the model with the constant λ_i to one with the energy dependent λ_i is demonstrated. By setting the energy dependence term b to zero (a constant λ_i), this model is successfully restored to the model in Ref. [22].

Table 4.1: Coefficients of Fourier Series Expansion of $V(t)$ for Varying b
$V_k = C'_k H(en_0\tilde{s}_0^2/\epsilon_0) = C_k H_0(en_0\tilde{s}_0^2/\epsilon_0)$

b	C'_0	C'_1	C'_2	C'_3
0	1.00	1.28	0.25	-0.034
0.1	1.02	1.30	0.25	-0.035
0.2	1.04	1.33	0.25	-0.037
0.3	1.06	1.35	0.25	-0.039
0.4	1.09	1.38	0.25	-0.041

b	C_0	C_1	C_2	C_3
0	1.00	1.28	0.25	-0.034
0.1	1.14	1.46	0.28	-0.039
0.2	1.31	1.67	0.31	-0.047
0.3	1.54	1.96	0.36	-0.057
0.4	1.84	2.33	0.42	-0.070

Table 4.2: Some Parameters for Varying b

b	H	s_m	$\bar{V}$	K	$V(0)$	V_1	V_2	V_3	C'_s	G'_s	$\bar{S}$	S_i
0	1.61	0.86	190	0.48	473	242	47.3	-6.43	0.15	1.43E-3	3.6E-3	6.3E-3
0.1	1.80	0.96	216	0.50	535	276	53.0	-7.38	0.14	1.27E-3	4.0E-3	7.2E-3
0.2	2.04	1.10	248	0.53	615	316	58.7	-8.89	0.12	1.12E-3	4.6E-3	8.2E-3
0.3	2.33	1.27	291	0.56	719	371	68.1	-10.8	0.10	9.70E-4	5.3E-3	9.7E-3
0.4	2.72	1.49	348	0.59	855	441	79.5	-13.2	0.087	8.26E-4	6.2E-3	1.2E-2

s_m - ion sheath thickness in cm; $\bar{V}$ - dc voltage across the sheath in V; K - coefficient in Child's law (Eq. 4.26); $V(0)$ - peak value of sheath voltage in V; V_1, V_2, and V_3 - first, second, and third harmonic of sheath voltage in V; C'_s - sheath capacitance in pF/cm^2; G'_s - sheath conductance in S/cm^2; $\bar{S}$ - average power transferred to electrons per unit area in W/cm^2; S_i - dc ion power flux incident on electrode in W/cm^2.

Chapter 5

IEDs in Collisional, Capacitive RF Sheath

5.1 Introduction

At high operating pressures, the rf sheaths are typically collisional with the ion mean free path much smaller than the sheath width. While traversing the sheath, ions have collisions with neutrals. Through an ion-neutral charge exchange collision, the ion is neutralized by picking up a unit charge from the neutral, and cannot be accelerated by electric field any more. The neutral loses a negative unit charge and becomes a secondary ion, with an initial energy of order the thermal energy of the background gas. The secondary ion then gets accelerated by the electric field. The final kinetic energy that an ion can carry to the substrate is smaller than the sheath voltage drop. Instead, their bombarding energy is determined by the position where their last collision takes place. The ion-neutral elastic scattering also contributes to the spread of the IED, as the kinetic energy that the primary ion carries gets redistributed angularly. During these processes, the electron-sheath edge is oscillating back and forth. Secondary ions generated by ion-neutral charge exchange collisions may be created within the space-charge region (between the instantaneous sheath edge and the electrode surface) or within the zero electric field region. Ions born within the space-charge region are accelerated immediately by the electric field in the sheath, while those born within the zero electri field region remain at rest until the oscillating sheath passes by. These ions experience a delay in their movement towards the electrode, which makes multiple peaks in the final IED. Due to ion-neutral collisions, combined with the effects of the oscillating sheath, the IED is broad and has multiple peaks at low energies.

The ion mean free path $\lambda_i = 1/n_g\sigma$ is a characteristic parameter in evaluating the collisional degree within the sheath. Here, n_g is the number density of neutrals, and σ is the cross section of the ion-neutral collision. Most of the existing models and numerical calculations of collisional rf sheaths assume λ_i is a constant, in order to simplify the problem.

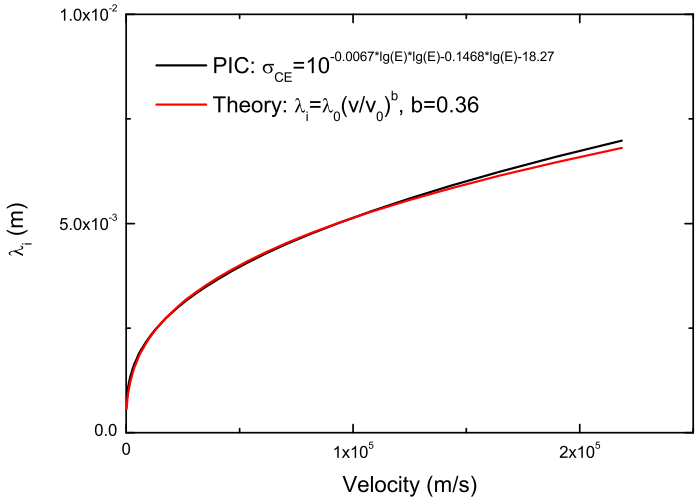

Figure 5.1: Ion mean free path λ_i vs. ion velocity

However, given the fact that the ion-neutral cross section is always energy dependent and for a typical capacitive rf discharge, the energy of ions within the sheath has a wide range from almost zero to the maximum sheath drop (hundreds of volts), the IED can be very sensitive to the cross section. In other words, an energy dependent ion mean free path is required to obtain accurate estimation of the IED. Fig. 5.1 gives an example of λ_i vs. ion velocity v_i employed in PIC simulations (data from experiments [39]). In PIC simulations, we specify the cross sections for ion-neutral charge exchange collisions as the black line shown in Fig. 5.1. Our theoretical model does not deal with the cross section σ directly, but assumes the ion mean free path is a function of ion velocity: $\lambda_i = \lambda_0(v_i/v_0)^b$, as shown in the red line. λ_0 is defined as the ion mean free path at a reference velocity v_0. Given that $\lambda_i = 1/n_g\sigma$, $b = 0.36$ gives a good fit for the ion-neutral collision probability between PIC and theory.

A newly developed collisional IED model, consisting of a series of fast computational steps, is described in this chapter. By acquiring the plasma parameters (time-varying sheath width and sheath voltage) from a collisional rf sheath model [22], this model predicts the IED numerically with only the control parameters required for the calculation. Section 5.2 describes the analytical model for high voltage rf capacitive discharges with collisional rf sheaths. In Section 5.3, the collisional IED model with energy dependent ion mean free path for ion-neutral charge exchange reactions, time-varying sheath voltage, and the oscillating sheath is developed to rapidly predict the IED within a collisional rf sheath. In Section 5.4, verifications of the sheath model and the IED model by PIC simulations are performed. Discussions and conclusions are presented. Summary and future work is presented in the last sections.

5.2 Collisional, Capacitive RF Sheath Model

In 1989, a simple analytical model of a collisional rf sheath was developed [22]. This model provides a self-consistent solution for the dynamics of a high-voltage, capacitive rf sheath driven by a sinusoidal current source. The ion motion is collisional, with the ion mean free path λ_i a constant within the sheath. It is assumed that the ions only respond to the time-averaged electric field, while the electrons respond to the instantaneous electric field. The ions enter the sheath with a Bohm velocity $u_B = (eT_e/M)^{1/2}$, with T_e the electron temperature (in Volts). Given the control parameters of a capacitive rf discharge, this model gives the time-averaged electric field and potential within the sheath, the nonlinear oscillation of the electron sheath boundary, and the nonlinear oscillating sheath voltage.

5.2.1 Example

Here is an example to explain how this collisional rf sheath model works to obtain the plasma parameters needed by the IED model. The capacitive rf discharge is driven by a single frequency voltage source $V(t) = V_{rf}\cos(2\pi ft)$ under pressure p in argon. The distance between electrodes is l and the area of the electrodes is A. The parameters used here are as follows: $V_{rf} = 176$ V, $f = 81$ MHz, $p = 20$ mTorr, $l = 0.024$ m, and $A = 5.03 \times 10^{-3}$ m^2. Ions are weakly collisional, with sheath width / ion mean free path $s_m/\lambda_0 \sim 1.1$, ion transit time across sheath / rf period $\tau_{ion}/\tau_{rf} \sim 10$.

Starting with an estimate of the ion sheath thickness $s_m \approx 0.0017$ m, and using $\lambda_i = 1/330p$ (p in Torr, λ in cm) at 300K, the ion mean free path in the sheath is $\lambda_i = 0.0015$ m. The plasma length $d \approx l - 2s_m = 0.0206$ m. $\lambda_i/d = 0.0736$, which is in the intermediate mean free path regime. The ratio between the edge density and center density is given by

$$h_l \equiv \frac{n_s}{n_0} \approx 0.86(3 + \frac{d}{2\lambda_i})^{-1/2} \tag{5.1}$$

We have $n_s/n_0 = 0.2747$. From $\frac{1}{n_g d_{eff}} = \frac{2}{n_g d}\frac{n_s}{n_0}$ where $n_g = 3.3 \times 10^{16} p$ (p in Torr, n_g in cm^{-3}), we get $n_g d_{eff} = 2.47 \times 10^{19}$ (in m^{-2}). Solving the particle balance using Fig. 10.1 (T_e versus $n_g d_{eff}$ for Maxwellian electrons in argon), or numerically, using the rate coefficient of reaction 2 in Table 3.3 in Ref. [23], we find $T_e \approx 2.8$ V. This gives $u_B = (eT_e/M)^{1/2} \approx 2.59 \times 10^3$ m/s. Introduce a coefficient H,

$$H = (\frac{2\lambda_i \tilde{s}_0}{\pi^2 \lambda_D^2})^{1/2} \tag{5.2}$$

where $\tilde{s}_0 = J_1/(e\omega n_s)$, J_1 is given by

$$J_1 \approx 1.52\omega\epsilon\frac{V_{rf}}{2}\frac{1}{s_m} \tag{5.3}$$

The sheath voltage can be written as a Fourier series

$$V_s(t) = \sum_{k=0}^{\infty} V_k \cos(k\omega t) \tag{5.4}$$

with $V_0 = \bar{V} = 1.00H(en_s\tilde{s}_0^2/\epsilon)$, $V_1 = 1.28H(en_s\tilde{s}_0^2/\epsilon)$, $V_2 = 0.25H(en_s\tilde{s}_0^2/\epsilon)$, $V_3 = -0.034H(en_s\tilde{s}_0^2/\epsilon)$. The higher harmonics ($s > 3$) are small and discarded.

From Figure 3.17 (ε_c versus T_e) in Ref. [23] where ε_c is the collisional energy loss per electron-ion pair created, we get $\varepsilon_c \approx 60$ V and $\varepsilon_c + \varepsilon_e' \approx 80$ V, where ε_e' is the kinetic energy lost per electron lost from the plasma with $\varepsilon_e' \approx 7.2T_e$. Estimating $\nu_m \approx K_{el}n_g$ with K_{el} given by the rate coefficient of reaction 1 in Table 3.3, we get $\nu_m \approx 6.6 \times 10^7$ s^{-1}. Then the electron ohmic heating power per unit area can be obtained by

$$\bar{S}_{ohm} \approx \begin{cases} 1.73\frac{m}{2e}\frac{n_s}{n_0}\epsilon_0\omega^2\nu_m T_e^{1/2}V_1^{1/2}d & \text{if } \lambda_i \geq (\frac{T_i}{T_e})d \\ 1.73\frac{m}{2e}\frac{n_s}{n_0}\epsilon_0\omega^2\nu_m T_e^{1/2}V_1^{1/2}\frac{2}{\beta}\ln\tan(\frac{\pi}{4}+\frac{\beta d}{4}) & \text{if } \lambda_i \leq (\frac{T_i}{T_e})d \end{cases} \tag{5.5}$$

where $\cos(\beta d/2) = n_s/n_0$, V_1 is the fundamental rf voltage amplitude across a single sheath. For our parameters, $\lambda_i \geq (\frac{T_i}{T_e})d$. Therefore, we obtain $\bar{S}_{ohm} \approx 63.25$ W/m^2. For the stochastic heating power per unit area,

$$\bar{S}_{stoc} \approx 0.61(\frac{m}{e})^{1/2}\epsilon_0\omega^2 T_e^{1/2}V_1 \quad \text{if } \omega s_m \leq \bar{v}_e \tag{5.6}$$

We get $\bar{S}_{stoc} \approx 449.25$ W/m^2. Similar to the derivation procedure in the collisionless model, we get $n_s \approx 1.58 \times 10^{16}$ m^{-3}, $n_0 \approx 5.74 \times 10^{16}$ m^{-3}, $\bar{J}_i \approx 6.00$ A/m^2, $s_m \approx 0.0016$ m (very close to the assumed value 0.0017 m), $S_{abs} \approx 1785.3$ W/m^2, $P = S_{abs} \times A = 8.98$ W. The fundamental current density is $J_1 \approx 353$ A/m^2. We have $H \approx 2.94$, $\bar{V} \approx 69.51$ V, $V_1 \approx 88.97$ V, $V_2 \approx 17.38$ V, $V_3 \approx -2.36$ V. The averaged ion-bombarding energy $\bar{\varepsilon}_i \approx 0.62\bar{V}\lambda_i/s_m = 38.03$ V. It is noted that $\bar{V}/V_1 \approx 0.78$, which agrees with the equation (11.2.56) in Ref. [23].

5.3 Collisional IED Model

5.3.1 Limitation

In this model, electrons are inertialess and respond to the instantaneous electric field; ions respond to the time averaged electric field. This model requires: $\omega_{pe} >> \omega_{rf} >> 1/\tau_{ion}$. Here, ω_{pe} is the electron plasma frequency, ω_{rf} is the rf frequency, and τ_{ion} is the ion transit time across one single sheath.

This collisional IED model takes into account ion-neutral charge exchange collisions. Elastic scattering between ions and neutrals is not considered here. The ion-neutral mean free path is energy dependent, with $\lambda_i = \lambda_0(v/v_0)^b$, where λ_0 is the ion mean free path

at a reference ion velocity v_0 corresponding to an ion temperature $T_i = 0.05$ V. We use $\lambda_0 = 1/(330p)$ in cm, p in Torr. b is the adjustable power in the $\lambda_i - v$ relation, which reveals the dependence of the charge exchange cross section on energy. For example, $b = 0$ gives a constant ion mean free path; the cross section data originally used in OOPD1 gives $b = 0.36$. The sheath voltage is time-varying, $V_s(t) = \bar{V}_s + \tilde{V}_s \sin(\omega_{rf} t)$. $\bar{V}_s$ is the time averaged sheath voltage over an rf period. $\tilde{V}_s$ is the amplitude of the oscillating part of sheath voltage. $\omega_{rf} = 2\pi f$, with f the rf frequency.

In this section, the sheath width $s(t)$ is assumed to be a constant with $s(t) = s_m$, which means that the sheath is not oscillating. In fact, the sheath is oscillating between a maximum thickness of s_m and a minimum thickness of a few Debye lengths λ_{De} from the electrode surface, as we will discuss in a subsequent section.

An expression for the oscillating sheath $s(t)$ is given in Ref. [16]. In their model, ion motion within the sheath is assumed to be weakly collisional, ion mean free path $\lambda_i >> s_m$, and the analysis is restricted to charge exchange collisions.

5.3.2 Scheme

We assume that a constant flux of ions coming from the bulk plasma enters the plasma-sheath edge at $x = 0$ at Bohm velocity u_B; ions are considered as two groups: the uncollided group and the collided group. The uncollided ions bombard the electrode with the total sheath voltage that they can pick up as they enter the plasma-sheath edge. Ions having charge exchange collisions within the sheath pick up the cold neutrals energy T_n and, as the secondary ions, are accelerated towards the electrode. The energy they take to the electrode is determined by their last charge exchange collision.

In our model, IEDs contributed from the uncollided and the collided ions are calculated separately. The uncollided IED is calculated from Benoit-Cattin's model[2], which can be considered as a collisionless sheath case. The collided IED is calculated from our IED model. Then the two parts of IEDs are combined through normalization of the total IED.

5.3.3 Example

Constant λ_i, constant V_s

In this case, $\lambda_i = \lambda_0$, $V_s(t) = \bar{V}_s$.

Let G_0 be the flux of ions (ions / m^{2}s) entering the plasma-sheath edge at $x = 0$. The total flux that hits the electrode at $x = s_m$ without having a collision is

$$\Gamma_0 = G_0 e^{-s_m/\lambda_0} \tag{5.7}$$

Now let $\Gamma_i(x)$ be the flux of ions having at least i collisions within the sheath.

Here, the concept of differential flux $\Gamma_i'(x)$ is used. For example, $\Gamma_1'(x)$ is the flux of ions having at least one collision within the sheath. It is known that,

$$d\Gamma_1(x) = \Gamma_0(x) n_g \sigma dx \tag{5.8}$$

where n_g is the neutral density, σ is the cross section of charge exchange collisions, and $\Gamma_0(x)$ is the flux of ions that do not have collisions before x. $d\Gamma_1(x)$ shows the increase of flux of the ions that have their first collision at x. Setting $\lambda_0 = \frac{1}{n_g \sigma}$, we have

$$d\Gamma_1(x) = \Gamma_0(x) \frac{1}{\lambda_0} dx \tag{5.9}$$

Since $d\Gamma_0(x) = -\Gamma_0(x)\frac{1}{\lambda_0}dx$, we have $\Gamma_0(x) = G_0 e^{-x/\lambda_0}$. With the initial condition $\Gamma_0 = G_0$ at $x = 0$, we get $\Gamma_0(x) = G_0 e^{-x/\lambda_0}$. Therefore, we have

$$d\Gamma_1 = G_0 e^{-x/\lambda_0} \frac{1}{\lambda_0} dx \tag{5.10}$$

Thus,

$$\Gamma_1'(x) = \frac{d\Gamma_1}{dx} = \frac{1}{\lambda_0} G_0 e^{-x/\lambda_0} \tag{5.11}$$

Integrating this differential flux from $x = 0$ to $x = s_m$ yields the total ion flux at the electrode that has had at least one collision within the sheath.

With the expression of $\Gamma_1'(x)$, we can get $\Gamma_2'(x)$, $\Gamma_3'(x)$, etc. in a similar way as shown in the following: Consider a position ξ within the sheath. $\Gamma_1'(\xi)d\xi$, which is $d\Gamma_1(\xi)$, shows the increase of the flux of ions lying between position ξ and $\xi + d\xi$. These ions have their first collision at ξ. This also shows the contribution of the ions transferring from the no-collision group to the at-least-one-collision group.

We have

$$d\Gamma_2(x) = \Gamma_2'(x)dx = \int_0^x \Gamma_1'(\xi) \frac{1}{\lambda_0} e^{-(x-\xi)/\lambda_0} d\xi dx \tag{5.12}$$

Here, $\Gamma_1'(\xi)d\xi \cdot \frac{1}{\lambda_0} \cdot dx$ is the typical expression of ions having collisions between x and $x + dx$ with $\frac{1}{\lambda_0}$ as the 'cross section part' $'n_g\sigma'$. The integration is from 0 to x because only when the first collision happens before x do these ions contribute to $d\Gamma_2(x)$. $e^{-(x-\xi)/\lambda_0}$ represents the probability that, after these ions have their first collision at ξ, they don't have any collision again from ξ to x until they reach the position x and have their second collision at x.

Note that we always use $d\Gamma_2(x)$, not $\Gamma_2(x)$. This is because $d\Gamma_2(x)$ shows the change of the flux of an ion group. Ions that have at least one collision include those having one and more than one collisions. To move to the question of how many ions have at least two collisions, we only need to count how many ions that have only one collision have another collision. It's not necessary to count the ions that have already had more than one collision, since this group will surely contribute to the at-least-two-collision group.

The above explanation is to help clarify the following relation between differential flux and ion energy distribution function. $d\Gamma_i(x)$ is the differential flux of ions that have exact i collisions in the sheath, not the 'at-least-i-collision'.

To extend the above equation to the i-th collision differential flux, we have

$$\Gamma'_i(x) = \int_0^x \Gamma'_{i-1}(\xi) \frac{1}{\lambda_0} e^{-(x-\xi)/\lambda_0} d\xi \tag{5.13}$$

If at position x, $d\Gamma_i(x)$ (which is also $\Gamma'_i(x)dx$) ions that just have their i-th collision at x don't have any collision until they hit the electrode (implying a factor of $e^{-(s-x)/\lambda}$), the energy they will carry to the electrode is what they obtain from being accelerated by the electric field from x to the electrode.

$$\Gamma'_i(x) dx e^{-(s_m-x)/\lambda_0} = -f_i(E) dE \tag{5.14}$$

The index i in f_i identifies the contribution of ions having i collisions in the sheath to the IED at the electrode.

For this simple case with constant ion mean free path λ_0 and constant sheath voltage $\bar{V}_s$, the IED can be obtained analytically by summing up f_i:

$$f(E) = \frac{G_0 s_m}{\lambda_0 \bar{V}_s} \exp\left(-\frac{s_m E}{\lambda_0 \bar{V}_s}\right) + G_0 \exp\left(-\frac{s_m}{\lambda_0}\right) \delta(E - \bar{V}_s) \tag{5.15}$$

The first and second terms on the right side of the equation represent the contribution to the IED of the collided ions and uncollided ions, respectively. With the time varying sheath voltage considered, the second term for the uncollided IED will be expanded from a monoenergetic δ function to a bimodal energy spread function. The corresponding expression of the uncollided IED from our model with a constant λ_i and time varying sheath voltage $V_s(t) = \bar{V}_s + \tilde{V}_s \sin(\omega t)$ agrees with the expression of f_E in Benoit-Cattion's model [2].

It should be noted that, in the above derivation, we use λ_i to stand for the ion-neutral mean free path for charge exchange reactions. However, if we consider λ_i as a function of energy, $\lambda_i = \lambda_0(v/v_0)^b$, λ in the above equations should be specified carefully. Take Eq. 5.13 for example. λ in $\frac{1}{\lambda}$ is the ion mean free path when the ion-neutral charge exchange reaction takes place at position x, while the λ in $e^{-(x-\xi)/\lambda}$ is the ion mean free path between ξ and x where ions don't have collisions. In Eq. 5.14, λ in $e^{-(s_m-x)/\lambda}$ is the ion mean free path between x and s_m. We need to distinguish λ if λ is considered as energy dependent. While moving toward the electrode, ions are accelerated and having collisions all the way. The varying energy implies a varying ion mean free path, which determines the collisional probability as ions cross the sheath. Therefore, in a general case with energy dependent ion mean free path, we need to obtain the expression of the IED numerically.

Energy dependent λ_i, time varying V_s

For a more general case of energy dependent ion mean free path λ_i and time varying sheath voltage V_s, we assume $\lambda_i = \lambda_0(v/v_0)^b$, $V_s(t) = \bar{V}_s + \tilde{V}_s \sin(\omega_{rf} t)$. Differing from the constant

λ_i case, energy conservation is needed for the energy dependent λ_i case to establish the relation between λ_i and V_s. Since V_s is time varying, discretization of V_s in time is needed to reflect the effects of the phase at which ions enter the plasma-sheath edge. In other words, by discretizing V_s in time, we are able to treat each discretized V_s as a constant and do the calculation in the same way as above for the constant V_s case.

It should be noted that the voltage that ions can actually feel and respond to becomes $V_i(t) = \bar{V}_s + \alpha\tilde{V}_s \sin(\omega_{rf}t)$. The averaged sheath voltage felt by ions does not change, but the amplitude of the oscillating sheath voltage shrinks by a factor of α. Here, α is the filter function in Ref.[45], $\alpha(f) = [(c2\pi f\tau_{ion})^q + 1]^{-1/q}$ with $c = 0.3 \times 2\pi$ and $q = 5$.

The uncollided ions carry the full voltage $V_i(t)$ to the electrode, the value of which is determined by the phase at which ions enter the plasma-sheath edge. The cases we consider in this model deal with $\tau_{ion} >> T_{rf}$, with T_{rf} an rf period. It takes a few rf periods for ions to cross the sheath. By doing an average of V_i over one rf period, we neglect the variation of V_i while the ions cross the sheath and take the value of V_i when ions first enter the plasma-sheath edge as the final energy they carry to the electrode. The same consideration of $V_i(t)$ is applied to the collided ions.

The differential flux in a general expression is as follows:

$$\Gamma'_i(x) = \int_0^x \frac{1}{\lambda_i}\Gamma'_{i-1}(\xi)e^{-\int_\xi^x \frac{1}{\lambda_i}d\eta}d\xi \tag{5.16}$$

The relation between differential flux and ion energy distribution function is as follows:

$$\Gamma'_i(x)dxe^{-\int_x^{s_m} \frac{1}{\lambda_i}d\eta} = -f_i(E(x))dE \tag{5.17}$$

To get a better understanding of Eq. 5.16 and Eq. 5.17, we consider the expression of $\lambda(x)$ for different cases.

(1) uncollided ions

The ion velocity is given by energy conservation

$$\frac{1}{2}Mv^2 = \frac{eV_i}{s_m}x + \frac{1}{2}Mu_B^2 \tag{5.18}$$

Here the Bohm velocity term is added to the initial energy conservation relation to account for the initial ion energy. Because of this correction of energy conservation, the expression of mean free path is corrected correspondingly as follows:

$$\lambda(x) = \lambda_0 \left(\frac{2eV_i}{Mv_0^2 s_m}\right)^{b/2} \left(x + \frac{Mu_B^2 s_m}{2eV_i}\right)^{b/2} \tag{5.19}$$

Setting $E_{u_B} = \frac{1}{2}Mu_B^2$, since $u_B = \sqrt{eT_e/M}$, we have $E_{u_B} = eT_e/2$. Setting $\delta = \left(\frac{E_{u_B}}{eV_i}\right)s_m$, $C_\lambda = \lambda_0 \left(\frac{eV_i}{E_{u_B}s_m}\right)^{b/2}$, and substituting in the above equation, we get

$$\lambda(x) = C_\lambda (x+\delta)^{b/2} \tag{5.20}$$

With these corrections, Eq. 5.9 should be

$$d\Gamma_1(x) = \Gamma_0(x) \frac{1}{C_\lambda (x+\delta)^{b/2}} dx \tag{5.21}$$

$\Gamma_0(x)$ should also be corrected to

$$\Gamma_0(x) = G_0 e^{-\int_0^x \frac{1}{\lambda(\xi)} d\xi} \tag{5.22}$$

with $\lambda(\xi) = C_\lambda(\xi+\delta)^{b/2}$. Therefore,

$$\Gamma_1'(x) = \frac{G_0}{C_\lambda (x+\delta)^{b/2}} e^{-\frac{1}{C_\lambda(1-b/2)}\left((x+\delta)^{1-b/2} - \delta^{1-b/2}\right)} \tag{5.23}$$

(2) collided ions

When ions have charge exchange reactions with neutrals, they pick up the kinetic energy of the background neutrals eT_n. Therefore, the correction of energy conservation for collided ions should be $eT_n = 0.026$ eV instead of E_{u_B}.

The ion velocity is given by energy conservation

$$\frac{1}{2} M v^2(x) = \frac{eV_i}{s_m}(x-\xi) + eT_n \tag{5.24}$$

where ξ is the position of the ion collision before it reaches the position x. We get

$$\lambda(x) = C_\lambda (x - \xi + \delta')^{b/2} \tag{5.25}$$

with $\delta' = \left(\frac{T_n}{V_i}\right) s_m$.

Similarly, Eq. 5.13 should be corrected as

$$\Gamma_i'(x) = \int_0^x \Gamma_{i-1}'(\xi) \frac{1}{C_\lambda (x-\xi+\delta')^{b/2}} e^{-\frac{1}{C_\lambda(1-b/2)}\left((x-\xi+\delta')^{1-b/2} - \delta'^{1-b/2}\right)} d\xi \tag{5.26}$$

Using Eq. 5.23 and Eq. 5.26 we can get all the differential fluxes.

To get the IED, we also need to correct Eq. 5.14. The energy conservation should be

$$\frac{1}{2} M v^2(\xi) = \frac{eV_i}{s_m}(\xi - x) + eT_n \tag{5.27}$$

with $x < \xi < s$. Therefore, λ in Eq. 5.14 should be

$$\lambda(\xi) = C_\lambda (\xi - x + \delta')^{b/2} \tag{5.28}$$

We have

$$\Gamma_i'(x) dx e^{-\frac{1}{C_\lambda(1-b/2)}\left((s_m+\delta')^{1-b/2} - (x+\delta')^{1-b/2}\right)} = -f_i(E) dE \tag{5.29}$$

5.3.4 Normalization

To normalize the total IEDs from both the uncollided and collided ions, we adjust the coefficient in the IED expression $f(E)$ in Benoit-Cattin's model. The probability of ions having at least one collision within the sheath, p_c, can be obtained by our model. Thus, $1-p_c$ should be the sum of the contribution of uncollided ions to the IED out of the total normalized IED. With the expression of $f(E)$ for the uncollided ions in Benoit-Cattin's model, we do the integral of $f(E)$ and let the integral equal to $1-p_c$, then we know what constant coefficient in $f(E)$ should be used. The total IED has been normalized through this procedure.

The contribution by uncollided ions to the IED can be obtained analytically by Benoit-Cattin's collisionless IED model[2]:

$$f(E) = (1-p_c)\frac{2}{\pi\Delta E}\left[1-\frac{4}{(\Delta E)^2}(E-\bar{V}_s)^2\right] \tag{5.30}$$

with $\Delta E = \frac{3\tilde{V}_s}{\pi}\left(\frac{\tau_{rf}}{\tau_{ion}}\right)$, and ion transit time across sheath $\tau_{ion} = 3\bar{s}/(2e\bar{V}_s/M)^{1/2}$.
The combination of IEDs contributed by uncollided and collided ions gives the final IED.

5.3.5 Notes

The sheath voltage $V_s(t)$ is discretized over half of an rf period, with nt the number of discrete grids. Note, here we discretize $V_s(t)$ over half of an rf period $(\pi/2, 3/2\pi)$, not an entire rf period, based on the fact that the behaviors of ions over the two halves of the rf periods are symmetric. Since $Vs(t)$ increases with time in $(\pi/2, 3/2\pi)$, discretization of IEDs over half of an rf period $(\pi/2, 3/2\pi)$ eliminates the sorting procedure required in normalizing the total IEDs. In other words, this is numerically preferred: when integrating the IEDs over energy, the sum can be done in a simple way.

The sheath width s_m is discretized differently in [0, $x1$] and [$x1$, s_m]. Here $x1$ is the position corresponding to the ion bombarding energy $\bar{V}_s - \Delta E/2$, and s_m is the position corresponding to the ion bombarding energy $\bar{V}_s + \Delta E/2$. ΔE is the energy width of the uncollided IEDs in Benoit-Cattin's model.

Collided ions bombard the electrode with energy ranging from zero to $V_i(t)$, with $V_i(t)$ varying from $\bar{V}_s - \Delta E/2$ to $\bar{V}_s + \Delta E/2$. Here $V_i(t)$ is the time-varying sheath voltage felt by the ions, which can be obtained by applying a filter α to the sheath voltage $V_s(t)$. For example, if $V_s(t) = \bar{V}_s + \tilde{V}_s \sin(\omega_{rf} t)$, then $V_i(t) = \bar{V}_s + \alpha\tilde{V}_s \sin(\omega_{rf} t)$. The averaged sheath voltage felt by ions does not change, but the amplitude of the oscillating sheath voltage shrinks by a factor of α. Here, $\alpha = 1/(1+(cf_{rf}\tau_{ion})^q)^{1/q}$, with $c = 2/3\pi$, $q = 2$, $\tau_{ion} = 3\bar{s}/(2e\bar{V}_s/M)^{1/2}$. $\bar{s}$ is the average sheath width[30, 45]. In Ref. [45], $c = 0.3 \times 2\pi$ is used in the semianalytical model in order to achieve a good agreement with PIC simulation results. Actually, the theoretical value of c should be $2\pi/3$, through which the uncollided IED obtained from this filter model

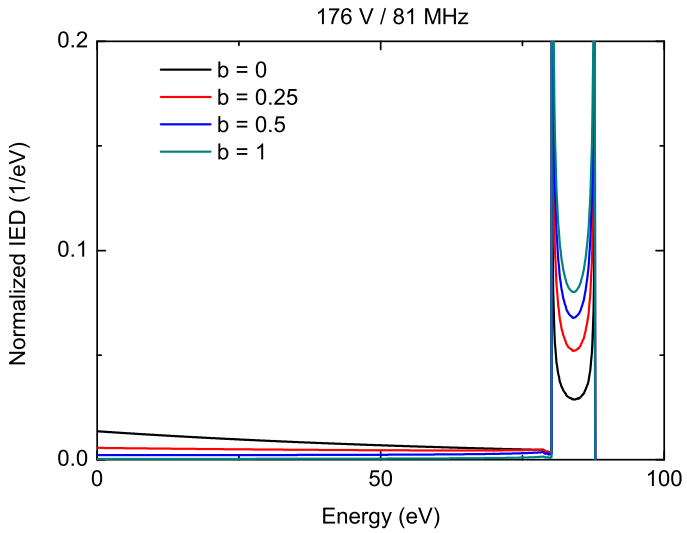

Figure 5.2: IED from theory at $V_{rf} = 176$ V with various energy dependence of λ_i over v

[45] agrees exactly with the IED in Benoit-Cattin's collisionless IED model [2], with the same IED spread and the same bimodal peaks.

For a discrete V_i, the IEDs contributed by the collided ions at this discrete time grid show a distribution over $(0, V_i)$. The sum of all the discrete distributions over $(0, V_i)$, with V_i from $\bar{V}_s - \Delta E/2$ to $\bar{V}_s + \Delta E/2$, makes the IEDs contributed by collided ions. We use a larger size step dx over $(0, \bar{V}_s - \Delta E/2)$ and smaller size step $dx1$ over $(\bar{V}_s - \Delta E/2, \bar{V}_s + \Delta E/2)$ in order to resolve the detailed IEDs and minimize the calculation cost.

The maximum number of charge exchange collisions considered in the model can be adjusted by the value of i. The choice of i can be roughly estimated from the ratio of sheath width s_m over ion mean free path λ_0.

The plasma parameters used in the code as the known values are obtained from the collisional sheath model [22], with a constant ion mean free path. The parameters employed here include: sheath width s_m, average sheath voltage $\bar{V}_s$ and amplitude of the oscillating sheath voltage $\tilde{V}_s$, and electron temperature T_e.

Differing from Benoit-Cattin's model that ions enter the sheath with zero initial velocity, in our model ions enter the sheath at Bohm velocity u_B. The secondary ions generated from charge exchange collisions have an initial kinetic energy eT_n, given by the cold neutrals at rest. These two corrections on the energy conservation relation of ions are necessary either from the aspect of revealing the true physics, or from the aspect of eliminating the possible singularity problem caused by a zero initial velocity.

Figure 5.2 shows the IEDs estimated by the collisional IED model at $V_{rf} = 176$ V, $f_{rf} = 81$ MHz, with various energy dependences of λ_i on velocity v. The black curve of

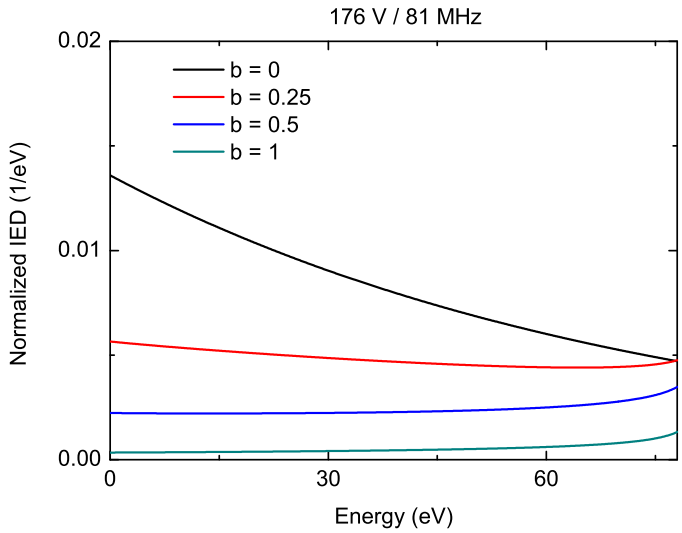

Figure 5.3: Collisional IED from theory at $V_{rf} = 176$ V with various energy dependence of λ_i over v

$b = 0$ is for constant λ_i, while the green curve of $b = 1$ represents a larger ion mean free path, which implies a less collisional sheath. As the value of b increases, λ_i increases, therefore the bimodal collisionless IED becomes more dominant since fewer ions have collisions as they cross the sheath. Details of the collisional part of the IEDs shown in Fig. 5.3 indicate that not only the absolute value of the collisional IEDs decreases as b increases, but also the trend of the curves changes: decreasing with ion bombarding energy E for smaller b, and increasing with E for larger b.

Another example of $V_{rf} = 500$ V at $f_{rf} = 13.56$ MHz is shown in Fig. 5.4. This case is more collisional than the $V_{rf} = 176$ V case. The results yield the same conclusion with the weakly collisional case of $V_{rf} = 176$ V referring to the effects of energy dependence of λ_i on the IED. The change exhibited in the collisional IEDs with various values of b, for both cases, confirms that it is valuable and necessary to consider λ_i as energy dependent when developing theoretical models and doing numerical calculations in collisional rf sheaths.

5.4 PIC Simulation

OOPD1 is used to verify the sheath model in Ref. [22] and the IED model in collisional rf sheaths.

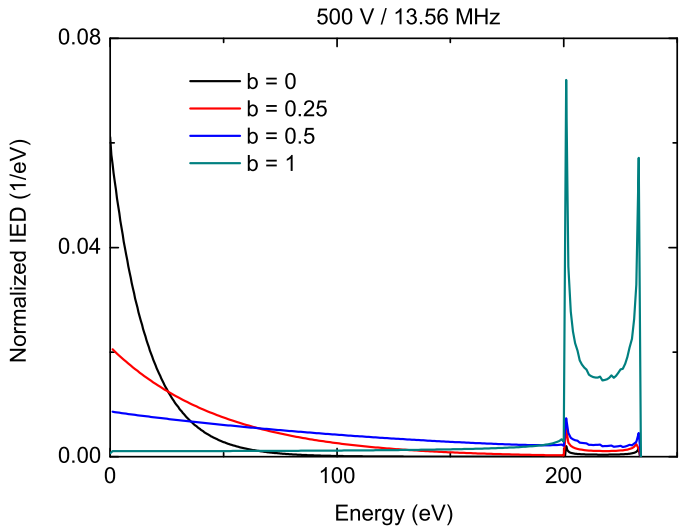

Figure 5.4: IED from theory at $V_{rf} = 500$ V with various energy dependence of λ_i over v

5.4.1 Verification of Collisional RF Sheath Model by PIC

The diagnostic of the sheath width in OOPD1 displays the oscillating sheath edge simultaneously. The sheath edge is defined at the position at which the ratio of time-averaged electron density over ion density reaches 0.8. The use of time-averaged densities and $n_e/n_i < 1$ is mainly due to the noisy oscillating sheath in the PIC simulation, as shown in Fig. 5.5. Doing a fast Fourier transform (FFT) on $s(t)$ in Fig. 5.5, we obtain the sheath width in frequency domain in Fig. 5.6. The first harmonic of the sheath width $s(t)$ is clearly shown with a peak at $f_{rf} = 81$ MHz.

Similarly, the diagnostic of the sheath voltage in OOPD1 displays the potential at plasma-sheath edge simultaneously. The sheath voltage V_s in time and frequency domains is shown in Fig. 5.7 and Fig. 5.8, respectively. The voltage driven capacitively coupled discharges exhibit a smoother sheath voltage, as shown in Fig. 5.7, while the current driven case will present a noisy sheath voltage with more harmonics. In all the existing theoretical models, including the collisionless and collisional rf sheath models [21, 22], Benoit-Cattin's collsionless IED model [2] and our IED models, only the first harmonic component of the sheath width and sheath voltage is assumed, with the secondary and higher harmonics discarded. Models in [21, 22] provide the method of choosing the amplitude of the first harmonic of $s(t)$ and $V_s(t)$, verified well by PIC simulations.

Figures 5.9, 5.10, and 5.11 present the time-averaged temperatures, potential, and number densities, respectively for $V_{rf} = 176$ V with $f = 81$ MHz at 20 mTorr. The input parameters required by the IED model, such as electron temperature T_e, time-averaged

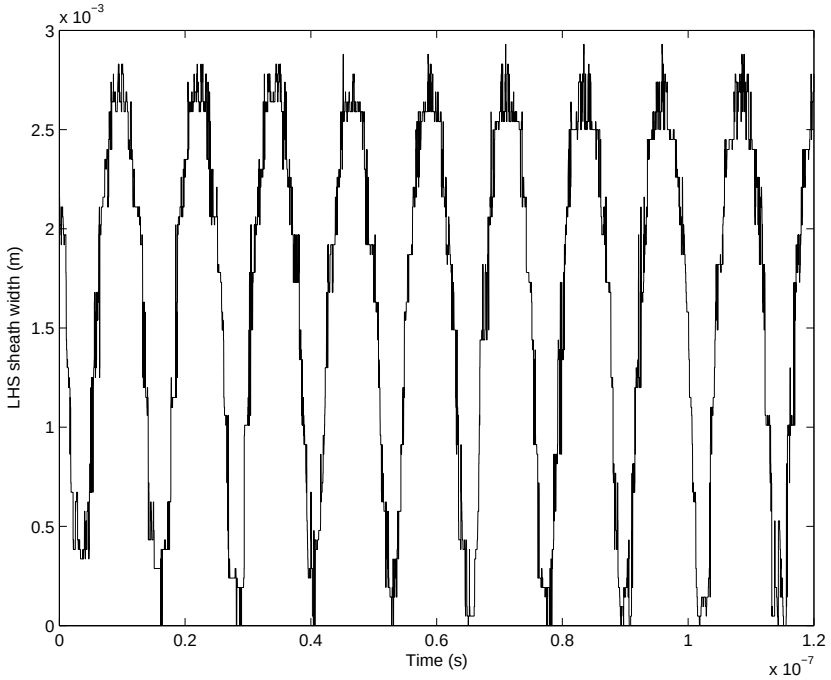

Figure 5.5: Sheath width vs. time

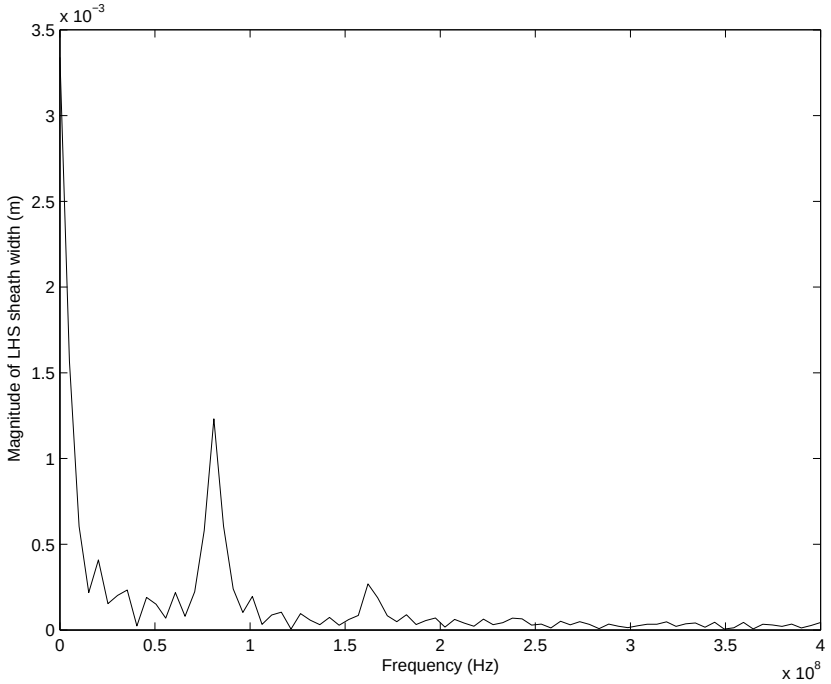

Figure 5.6: Magnitude of sheath width vs. frequency

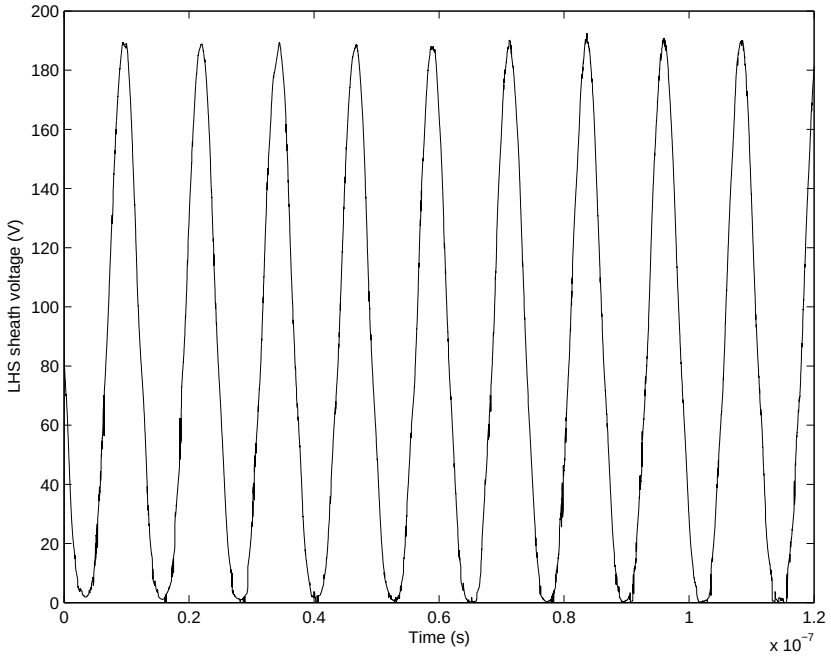

Figure 5.7: Sheath voltage vs. time

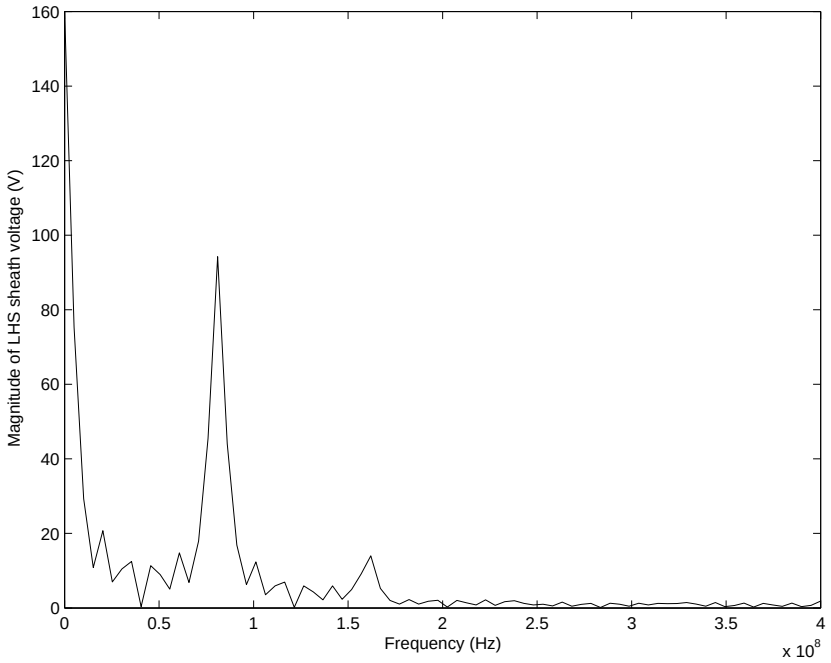

Figure 5.8: Magnitude of sheath voltage vs. frequency

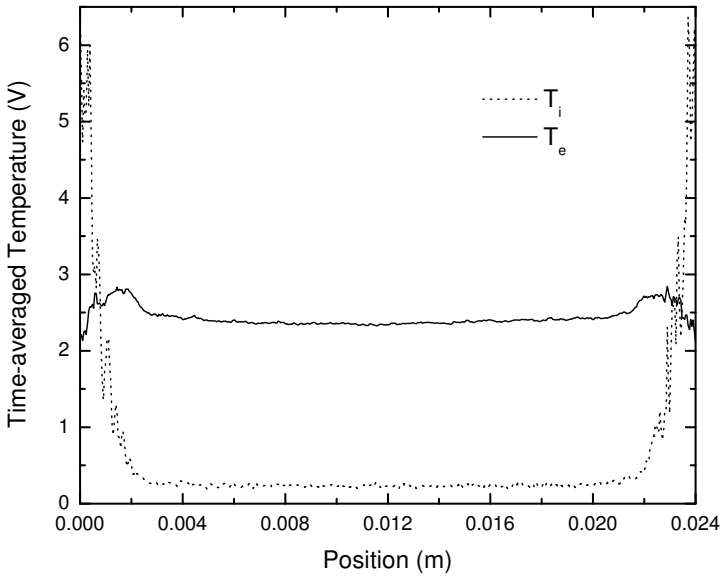

Figure 5.9: Time-averaged temperature vs. position

sheath voltage $\bar{V}_s$, and number density at plasma-sheath edge n_s, which are theoretically calculated by the collisional sheath model [22], are verified to be in good agreement with theory through these diagnostics in PIC simulations. It is shown in Fig. 5.11 that a large pre-sheath region exists before the number densities of electrons and ions branch. Within the sheath, the densities decrease gradually from the plasma-sheath edge to the electrode, which indicates that a homogeneous sheath model is far from an accurate estimation of the dynamics in the sheath. A collisional sheath model with densities satisfying the Child-Langmuir law can improve the model of the sheath dynamics.

Figure 5.12 shows the IED from PIC for $V_{rf} = 176$ V with $f = 81$ MHz at 20 mTorr. As shown in the figure, this is a weakly collisional case, with only a small fraction of ions undergoing ion-neutral collisions. The high peak near the time-averaged sheath voltage is contributed by ions having no collisions within the sheath, together with ions that have their last collisions very near the plasma-sheath edge.

5.4.2 PIC Results of Collisional IEDs

Figure 5.13 shows the IEDs from PIC at $V_{rf} = 500$ V with f_{rf} =13.56 MHz (red) and 27.12 MHz (black). With a fixed rf driving voltage, as the rf frequency doubles, the sheath width halves correspondingly. Therefore, the ions for 13.56 MHz case undergo more collisions

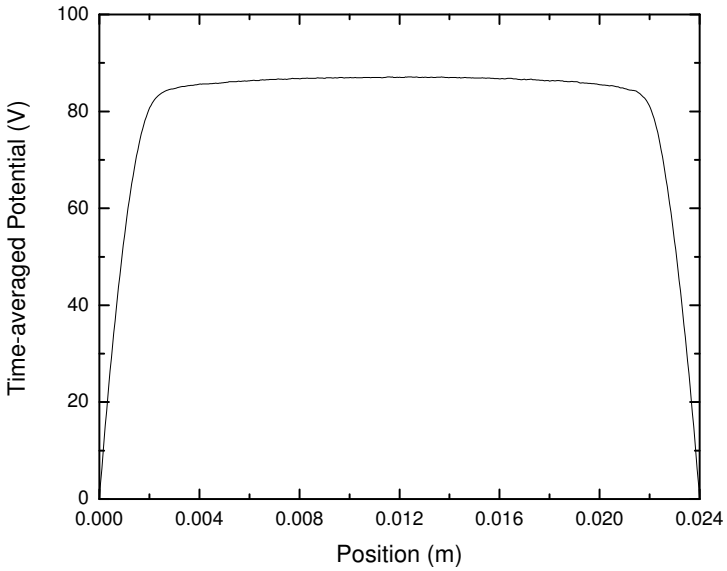

Figure 5.10: Time-averaged potential vs. position

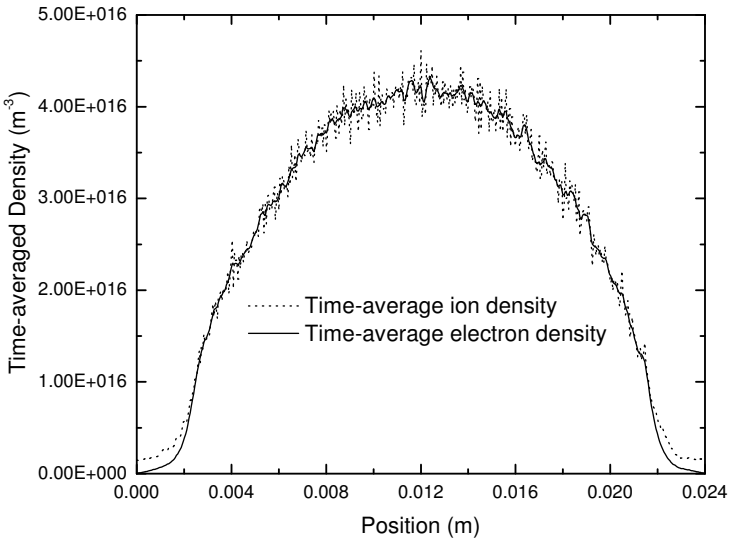

Figure 5.11: Time-averaged density vs. position

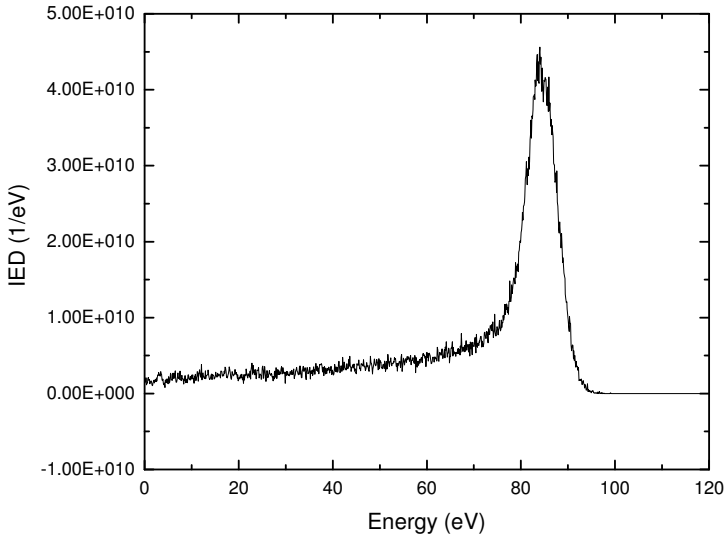

Figure 5.12: IED from PIC at $V_{rf} = 176$ V with f =81 MHz

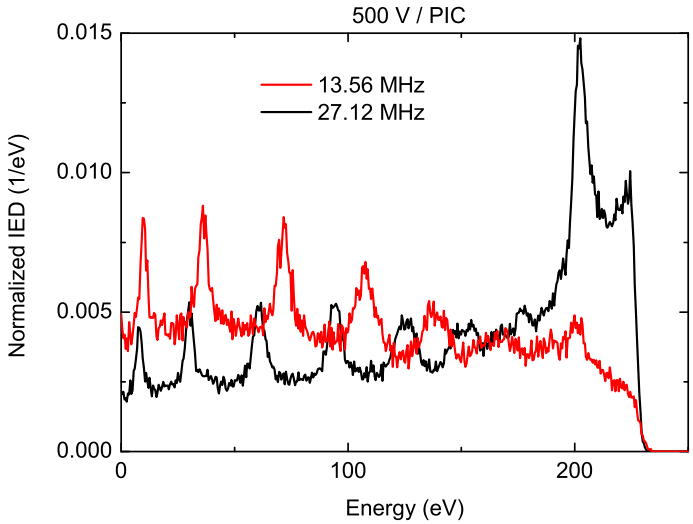

Figure 5.13: IEDs from PIC at $V_{rf} = 500$ V with f =13.56 and 27.12 MHz

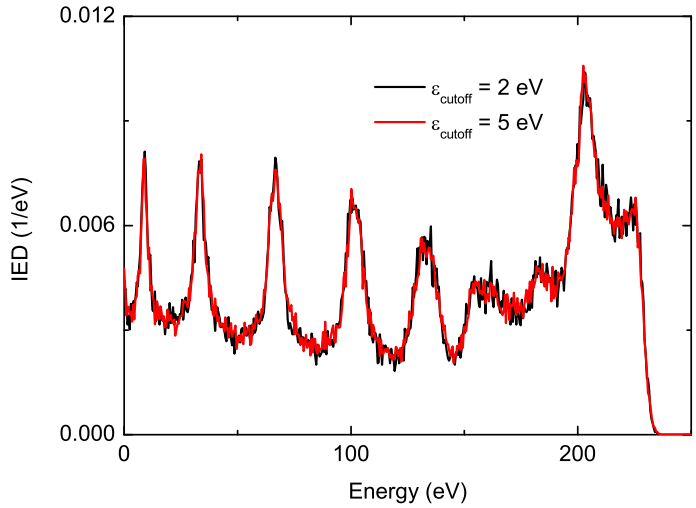

Figure 5.14: IED from PIC with different cutoff energies of fast neutrals ε

within the sheath, which explains the high peak in the IED for the 27.12 MHz case while the 13.56 MHz case exhibits more contributions from the collided ions in the low energy regime. Although the driving frequency varies, the ratio of ion transit time over the rf period τ_{ion}/τ_{rf} remains the same, which determines the number of peaks in the low energy regime in the IED. Therefore, the same number of peaks in the low energy regime contributed by collided ions is observed for both rf driving frequencies. This conclusion, also observed in the collisionless IED model and explained by Benoit-Cattin's IED model[2], can apply to a collisional sheath as well.

In PIC simulations, fast neutrals are specified as a separate particle group to investigate the behavior of fast neutrals. Given the fact that there are numerous background neutrals in the discharge, a cutoff energy is chosen to distinguish the fast neutrals from the background neutrals. A lower cutoff energy requires more computational resources in PIC simulations. Figure 5.14 shows the IEDs for $V_{rf} = 500$ V at $f_{rf} = 13.56$ MHz with different cutoff energies of fast neutrals. PIC results show that a 5 eV cutoff energy gives as good a description of the IEDs as a 2 eV cutoff energy does, while saving nearly half of the computational time. We use the 5 eV cutoff energy for all the related observations in this thesis. Obviously, differences will be seen in the neutral energy distribution (NED) with different cutoff energies for fast neutrals. Since our IED model does not take into account the ion-neutral elastic scattering, the ion-neutral elastic scattering collisions are turned off in PIC simulations in order to more accurately verify our IED model. A comparison of IEDs from PIC with and without ion-neutral elastic scattering considered is made. Results are shown in Fig. 5.15. The high peaks of IEDs contributed by the uncollided ions within the sheath are reduced by the ion-neutral

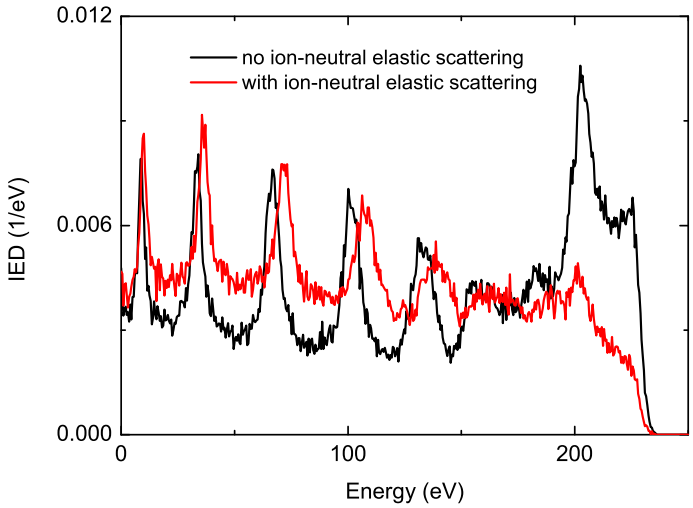

Figure 5.15: IED from PIC with/out ion-neutral elastic scattering collisions

elastic scattering collisions. Higher collisional IEDs are observed in the low energy regime with the elastic scattering considered, as expected. A slight shift of the multiple peaks due to elastic scattering is observed as well. Ion angular distributions (IADs) within the sheath are shown in Fig. 5.16. At the center of bulk plasma, the IAD is primarily isotropic. Within the sheath, ions are accelerated by the electric field towards the electrode. Therefore, the IADs are highly directed to the electrode within the sheath. The closer the observation position is to the electrode, the more directed are the ions to the electrode by the electric field. IEDs within the sheath suggest that the total energy spread ΔE is proportional to the distance from the plasma-sheath edge, as shown in Fig. 5.17.

5.4.3 Comparisons between theory and PIC

Results from theory and PIC are compared. The IEDs from theory (red) and PIC (black) are shown in Fig. 5.18 for $V_{rf} = 176$ V, $f_{rf} = 81$ MHz. Results show a good agreement of the energy spread in collisionless IED regime between theory and PIC. Another example of $V_{rf} = 500$ V is given in Fig. 5.19. As we can see from the figure, the maximum bombarding energy and the energy spread of the collisionless IED agrees well between theory and PIC. Due to the limitation of constant sheath width in our model, no multiple peaks are seen in the low energy regime. Figures 5.20 and 5.21 show the IEDs from theory and PIC with a constant λ_i and an energy dependent λ_i ($b = 1$), respectively. Results show good agreement between theory and PIC with respect to the energy spread and the peak position.

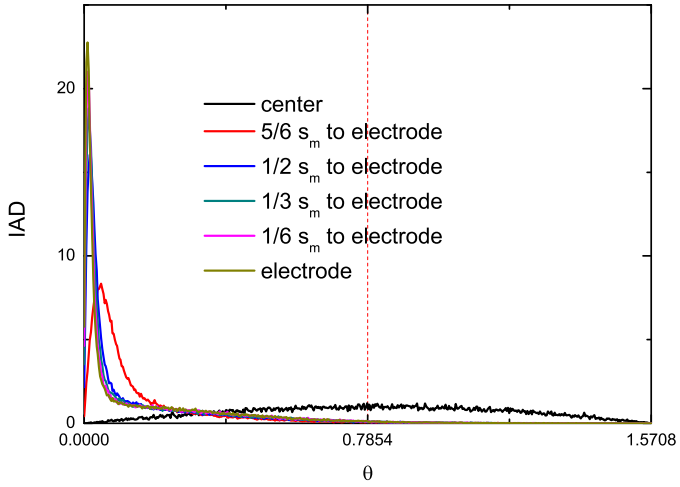

Figure 5.16: IADs within sheath, from PIC

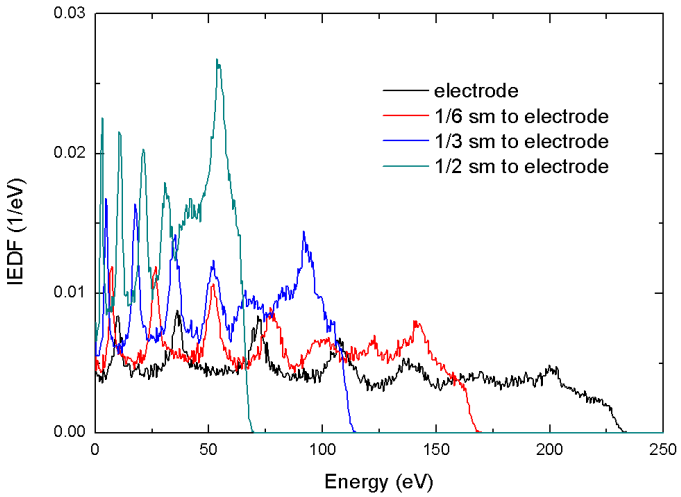

Figure 5.17: IEDs within sheath, from PIC

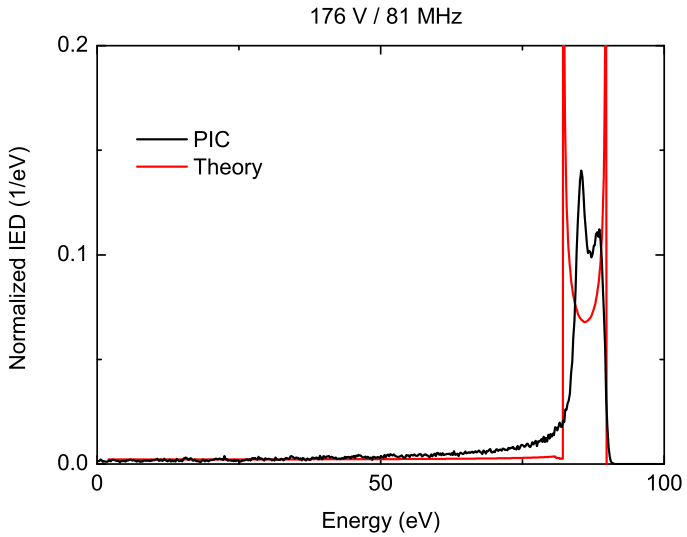

Figure 5.18: IEDs from theory and PIC at $V_{rf} = 176V$

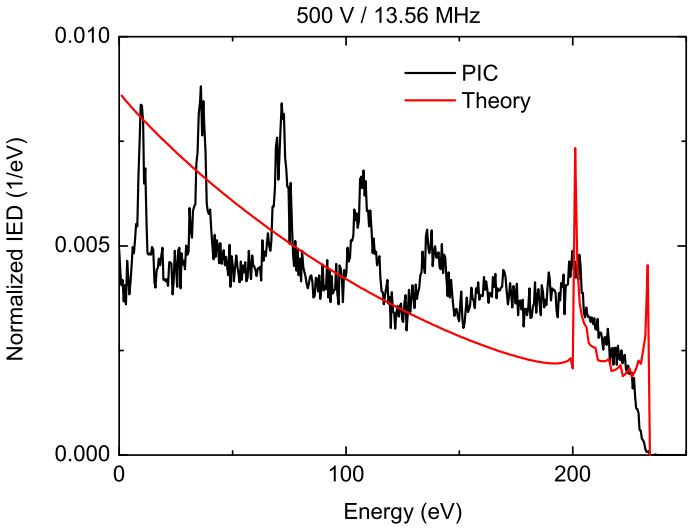

Figure 5.19: IEDs from theory and PIC at $V_{rf} = 500V$

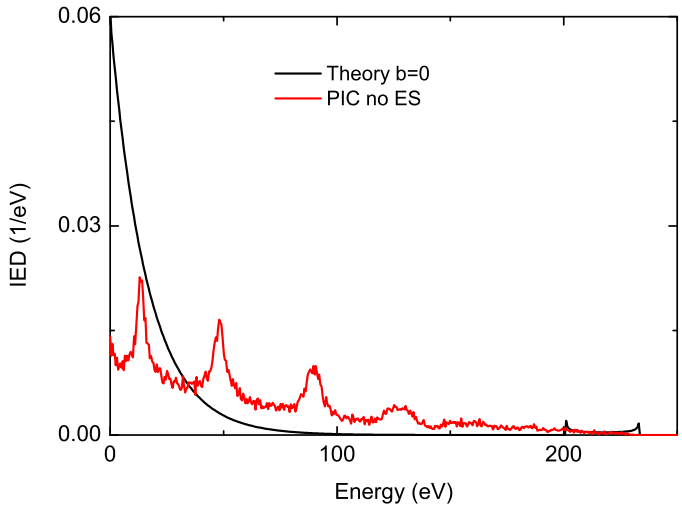

Figure 5.20: IEDs from theory and PIC with a constant λ_i

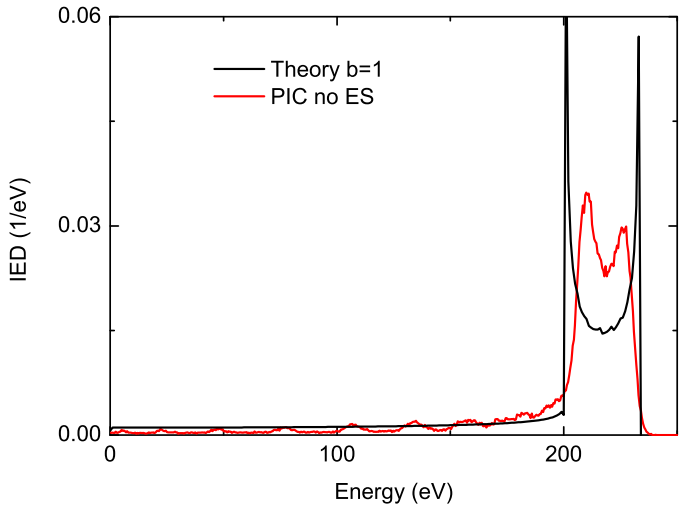

Figure 5.21: IEDs from theory and PIC with an energy dependent λ_i

5.5 Summary

A collisional IED model is developed with energy dependent ion-neutral charge exchange collisions, time-varying sheath voltage, and oscillating sheath. A collisional sheath model is used to calculate the plasma parameters required by the IED model. PIC simulations are run to verify the theory, finding good agreement, excluding the multiple peaks in the low energy regime, due to the limitation of the IED model.

5.6 Future Work

The collisional sheath model is developed under the assumption of a constant ion mean free path λ_i. With the energy dependence of λ_i taken into account, it is necessary and valuable to redo the collisional sheath model. This also provides another perspective to the calculation of IEDs. An updated sheath model in a collisional rf sheath with energy dependent ion mean free path, combined with Wencong Chen's collisional IED model [5], would probably make the accurate estimation of the IEDs achievable.

Chapter 6

Conclusion and Future Work

6.1 Conclusion

In this dissertation, the collisionless sheath model [21] and the collisional sheath model with a constant ion mean free path [22] is verified by PIC simulations with good agreement, for capacitive rf discharges. The sheath models estimate the input plasma parameters needed by the IED models. A collisional sheath model with the energy-dependent ion mean free path is developed. Effects of the dependence on the plasma parameters are investigated, showing that the plasma parameters are sensitive to the energy dependence of the ion mean free path, in other words, the cross section. A constant ion mean free path, as assumed in most of the existing models, is not accurate in studying the sheath dynamics and predicting the IED. An energy-dependent ion mean free path is required in the collisional rf sheath modeling.

The IED models, both for collisionless and collisional rf sheaths, are developed. A fast computational method of predicting the IEDs in collisionless and collisional rf sheaths is achieved. Combined with the sheath models which provides the needed plasma parameters for the IED models, the IEDs are obtained with only the control parameters (rf driving voltage or current, driving frequency, pressure, gas type, geometry) given, not relying on any intermediate parameters from experiments and simulations. PIC simulations are used to verify the IED models and find good agreement with the models.

The PIC code OOPD1 is introduced with powerful capability, fast speed, and user-friendly input. Neutral energy and angular distributions (NEDs and NADs) in collisional, capacitive rf sheaths are observed by OOPD1.

Fast theoretical models are valuable in plasma processing, especially when dealing with plasma behaviors within the sheath where it is difficult to measure the parameters in experiments. Although PIC simulations are fast compared to the experiments, a few days or weeks may be the normal computational cost. By using PIC simulations to verify the theory, one is able to study capacitive rf sheaths with some simple and fast theoretical models, which

provides the capability of understanding the physics of the sheath dynamics.

6.2 Future Work

The collisional IED model developed in this dissertation takes into account the ion-neutral charge exchange collisions. The ion-neutral elastic scattering collisions are not considered. Models including both ion-neutral reactions will predict the IEDs more accurately.

Although the oscillating sheath is included in the collisional IED model, with the sheath width discretized in time to reflect the oscillation, its effects on the IEDs are taken as an average. The motion of ions within the sheath does not respond to the oscillating motion of the sheath. This limitation makes the collisional IED model unable to show the multiple peaks in the IEDs at the low energies. Using the collisional sheath model with energy dependent ion mean free path, described in Chapter 4, together with Wencong Chen's collisional IED model [5], an accurate estimation of the IEDs may be achievable, with the multiple peaks clearly shown at the low energies.

The development of theoretical models for predicting the IADs, NEDs, and NADs in collisional rf sheaths are needed.

Bibliography

[1] M. S. Barnes, J. C. Forster, and J. H. Keller. In: *IEEE Trans. Plasma Sci.* 19 (1991), p. 240.

[2] P. Benoit-Cattin and L.-C. Bernard. In: *J. Appl. Phys.* 39 (1968), p. 5723.

[3] F. X. Bronold et al. In: *J. Phys. D: Appl. Phys.* 40 (2007), p. 6583.

[4] C. Charles, R. W. Boswell, and R. K. Porteous. In: *J. Vac. Sci. Technol. A* 10 (1992), p. 398.

[5] W. C. Chen et al. In: *Appl. Phys. Lett.* 94 (2009), p. 211503.

[6] R. T. Farouki, S. Hamaguchi, and M. Dalvie. In: *Phys. Rev. A* 45 (1992), p. 5913.

[7] D. Field et al. In: *J. Appl. Phys.* 70 (1991), p. 82.

[8] V. Georgieva, A. Bogaerts, and R. Gijbels. In: *Phys. Rev. E* 69 (2004), p. 026406.

[9] V. A. Godyak and N. Sternberg. In: *Phys. Rev. A* 42 (1990), p. 2299.

[10] W. J. Goedheer. In: *Plasma Sources Sci. Technol.* 9 (2000), pp. 507–516.

[11] R. A. Gottscho. In: *J. Vac. Sci. Technol. B* 11 (1993), p. 1884.

[12] Z. Q. Guan, Z. L. Dai, and Y. N. Wang. In: *Phys. Plasmas* 12 (2005), p. 123502.

[13] J. T. Gudmundsson. *Notes on the electron excitation rate coefficients for argon and oxygen discharge*. Tech. rep. RH-21. University of Iceland, 2002.

[14] W. M. Holber and J. Forster. In: *J. Vac. Sci. Technol. A* 8 (1990), p. 3720.

[15] J. Hopwood. In: *Appl. Phys. Lett.* 62 (1993), p. 940.

[16] D. Israel and K.-U. Riemann. In: *J. Appl. Phys.* 99 (2006), p. 093303.

[17] E. Kawamura et al. In: *Plasma Sources Sci. Technol.* 8 (1999), R45–R64.

[18] M. J. Kushner. In: *J. Appl. Phys.* 58 (1985), p. 4024.

[19] J. K. Lee et al. In: *IEEE Trans. Plasma Sci.* 32 (1 2004), p. 47.

[20] Y. D. Lee et al. In: *Phys. Plasmas* 7 (2000), p. 766.

[21] M. A. Lieberman. In: *IEEE Trans. Plasma Sci.* 16 (1988), p. 638.

[22] M. A. Lieberman. In: *IEEE Trans. Plasma Sci.* 17 (1989), p. 338.

[23] M. A. Lieberman and A. J. Lichtenberg. 2nd ed. New York: Wiley, 2005. Chap. 11.

[24] J. Liu, G. L. Huppert, and H. H. Sawin. In: *J. Apply. Phys.* 68 (1990), p. 3916.

[25] Z.-L. Liu and X.-B. Jing ang K.-L. Yao. In: *J. Phys. D* 38 (2005), p. 1899.

[26] A. Manenschijn and W. J. Goedheer. In: *J. Appl. Phys.* 69 (1991), p. 2923.

[27] K. Matyash et al. In: *Contrib. Plasma Phys.* 47 (2007), p. 595.

[28] P. W. May, D. Field, and D. F. Klemperer. In: *J. Appl. Phys.* 71 (1992), p. 3721.

[29] A. Metze, D. W. Ernie, and H. J. Oskam. In: *J. Appl. Phys.* 65 (1989), p. 993.

[30] P. A. Miller and M. E. Riley. In: *J. Appl. Phys.* 82 (1997), p. 3689.

[31] D. S. Nikandrov and L. D. Tsendin. In: *Tech. Phys. Lett.* 32 (2006), p. 719.

[32] D. O'Connell et al. In: *Phys. Plasmas* 14 (2007), p. 103510.

[33] M. Olevanov et al. In: *Phys. Rev. E* 78 (2008), p. 026404.

[34] T. Panagopoulos and D. J. Economou. In: *J. Appl. Phys.* 85 (1999), p. 3435.

[35] M. Surendra and D. B. Graves. In: *IEEE Trans. Plasma Sci.* 19 (1991), p. 144.

[36] Yoshinori Takao et al. In: *Jpn. J. Appl. Phys.* 50 (2011), 08JC02.

[37] B. E. Thompson, H. H. Sawin, and D. Fischer. In: *J. Appl. Phys.* 63 (1988), p. 2241.

[38] R. T. C. Tsui. In: *Phys. Rev.* (1968), p. 168.

[39] V. Vahedi and M. Surendra. In: *Comput. Phys. Commun.* 87 (1995), p. 179.

[40] D. Vender and R. W. Boswell. In: *IEEE Trans. Plasma Sci.* 18 (1990), p. 725.

[41] J. P. Verboncoeur. In: *Plasma Phys. Control. Fusion* 47 (2005), A231.

[42] J. P. Verboncoeur et al. In: *J. Comput. Phys.* 104 (1993), p. 321.

[43] C. Wild and P. Koidl. In: *Appl. Phys. Lett.* 54 (1989), p. 505.

[44] C. Wild and P. Koidl. In: *J. Appl. Phys.* 69 (1990), p. 2909.

[45] Alan C. F. Wu, M. A. Lieberman, and J. P. Verboncoeur. In: *J. Appl. Phys.* 101 (2007), p. 056105.

[46] N. Xiang and F. L. Waelbroeck. In: *Phys. Plasmas* 12 (2005), p. 033505.